IDH2 lactylation regulates mitochondrial dysfunction injury induced by myocardial ischemia-reperfusion via the AMPK signaling pathway

CHANGSEN WANG[1,2*], SIMAN SHEN[1*], SUYUN CHEN[1*], JINDA LIN[1], SIMENG LI[1], JIANNING CHEN[1], SHUYUN CAI[1], XIAODONG YUAN[1], ZIQIANG YANG[1], KUN DING[1], LI XU[3] and LIANGQING ZHANG[1]

[1]Department of Anesthesiology, The Second Affiliated Hospital of Guangdong Medical University, Zhanjiang, Guangdong 524003, P.R. China; [2]Department of Anesthesiology, Affiliated Hospital of Guangdong Medical University, Zhanjiang, Guangdong 524003, P.R. China; [3]Department of Laboratory Medicine, The Second Affiliated Hospital of Guangdong Medical University, Zhanjiang, Guangdong 524003, P.R. China

Received September 6, 2025; Accepted March 26, 2026

DOI: 10.3892/ijmm.2026.5833

Abstract. Ischemic cardiomyopathy ranks as a principal cause of death and incapacity worldwide. Myocardial ischemia-reperfusion injury (MIRI) caused by percutaneous coronary intervention is a major threat in the treatment of ischemic cardiomyopathy. Although lactylation (Kla) is extensively implicated in numerous pathological processes, its role and specific effects in MIRI remain unclear. Lactylation proteomics was used to identify proteins with different modifications during ischemia-reperfusion injury. Co-immunoprecipitation experiments were utilized to detect isocitrate dehydrogenase 2 (IDH2) lactylation levels. Immunofluorescence staining was applied to confirm intracellular lactylation levels. TUNEL, DHE and MitoSOX staining were used to measure oxidative damage in cells and tissues. An oxygen consumption rate experiment and the ATP assay were conducted to determine mitochondrial function. Western blots were utilized to detect changes in proteins related to mitochondrial functional homeostasis and downstream signal alterations. Excessive lactate accumulation was observed in MIRI model mice. This accumulation exacerbated the decline in cardiac function and the damage to cardiomyocytes in mice after MIRI. The lactylation of IDH2 in mitochondria was found to play a regulatory role in mitochondrial dysfunction and MIRI. Regarding the mechanism, it was verified that high IDH2 K275 lactylation caused a reduction in its enzymatic activity and decreased the production of α-ketoglutarate in the tricarboxylic acid cycle. Consequently, the activation of the AMPK pathway was inhibited, and mitochondrial damage and functional impairment were aggravated. It was also found that SIRT3 regulated and prevented IDH2 lactylation. The results of the present study indicated that IDH2 lactylation, which is elevated due to lactate accumulation and negatively regulated by SIRT3, contributes to the exacerbation of MIRI by regulating the functional homeostasis of mitochondria. This discovery offers a new therapeutic concept and target for MIRI prevention.

Correspondence to: Professor Liangqing Zhang, Department of Anesthesiology, The Second Affiliated Hospital of Guangdong Medical University, 12 Minyou Road, Xiashan, Zhanjiang, Guangdong 524003, P.R. China
E-mail: zhangliangqing@gdmu.edu.cn

Dr Li Xu, Department of Laboratory Medicine, The Second Affiliated Hospital of Guangdong Medical University, 12 Minyou Road, Xiashan, Zhanjiang, Guangdong 524003, P.R. China
E-mail: xulicmu@163.com

*Contributed equally

Abbreviations: MIRI, myocardial ischemia-reperfusion injury; PTM, post-translation modification; DCA, dichloroacetic acid; NaLac, sodium lactate; 8-OHdG, 8-hydroxy-2'-deoxyguanosine; DHE, dihydroethidium; IDH2, isocitrate dehydrogenase 2; DRP1, dynamin-related protein 1; MnSOD2, manganese superoxide dismutase 2; Cyt C, cytochrome C; SIRT3, sirtuin 3; α-KG, α-ketoglutaric acid; AAV9, adeno-associated virus 9; ROS, reactive oxygen species; NADPH, nicotinamide adenine dinucleotide phosphate; AMPK, adenosine 5'-monophosphate-activated protein kinase; CK-MB, creatine kinase-MB; 3-TYP, 3-(1H-1,2,3-Triazol-4-yl) pyridine; LVEF, left ventricular ejection fraction; LVFS, left ventricular fractional shortening

Key words: MIRI, lactylation, IDH2, mitochondrial dysfunction, SIRT3

Introduction

Despite current treatments, ischemic heart disease is the primary cause of global morbidity and mortality (1). Although thrombolysis or revascularization can effectively mitigate myocardial ischemic injury, the subsequent reperfusion can cause severe damage. This reperfusion-induced injury can account for up to 50% of the final myocardial infarction area and contribute to adverse events such as arrhythmia and cardiac arrest (2). The pathogenic mechanisms of ischemia-reperfusion

(I/R) injury include myocardial inflammation, apoptosis, calcium overload, excessive production of reactive oxygen species (ROS), and disturbances in energy metabolism (3). However, therapeutic targets must be identified and applied to facilitate recovery. Therefore, exploring the mechanisms of myocardial I/R injury (MIRI) and developing preventive and therapeutic measures are of clinical significance.

Mitochondria are the energy supply and metabolic hubs of cells and have been a major focus of cardiovascular research (4). Studies indicate that mitochondrial dysfunction is one of the key mechanisms by which mitochondria are implicated in I/R injury (5). The ATP balance of cardiomyocytes is typically maintained by mitochondria through oxidative phosphorylation (OXPHOS). However, during ischemia, hypoxia shifts energy production from OXPHOS to glycolysis, impairing ATP synthesis. Furthermore, an abrupt influx of oxygen results in a surge of ROS. ROS disrupt mitochondrial structure, damage mitochondrial membranes, respiratory chai and mitochondrial DNA (6). In contrast to conventional perspectives, emerging evidence suggests that mitochondrial dynamics are central to metabolic regulation. Mitofusin proteins 1/2 (MFN1/2) dynamically remodel mitochondrial architecture to form interconnected networks for content sharing and segregate damaged components by fusion with dynamin-related protein 1 (DRP1) (7,8). This dynamic equilibrium critically regulates energy efficiency and oxidative stress tolerance. Furthermore, PINK1/Parkin pathway-mediated impaired mitophagy is directly associated with Parkinson's disease and diabetes (9).

Mitochondria also act as signaling hubs by releasing ROS, calcium ions and metabolites, including acetyl-CoA and α-ketoglutarate (α-KG), to regulate nuclear epigenetic modifications and gene expression (10). For instance, mitochondrial-derived ROS and metabolites can activate oncogenic pathways or disrupt insulin signaling, connecting mitochondrial dysfunction to tumor progression and metabolic disorders (11). Therefore, mitochondrial research holds significant potential. A thorough investigation of the mechanisms regulating mitochondrial homeostasis is conducive to the development of more effective therapeutic strategies. Studies have demonstrated that mitochondrial function can induce abnormal flux changes in glycolysis and reprogram cell metabolism (11). Recently, it has been indicated that changes in glycolytic activity can regulate mitochondrial physiology through negative feedback mechanisms (12). However, the molecular mechanisms and physiological consequences of this bidirectional dialogue remain largely unexplored.

In addition to its role as a glycolytic end-product, lactate is now recognized as an important mediator and a substrate for a novel post-translational modification: Lactylation (13). This epigenetic mark, formed when lactate is covalently attached to lysine residues, is driven by intracellular lactate levels and regulated by 'writers' (for instance, P300/CBP) and 'erasers' [such as histone deacetylase (HDAC)]. In lactylation, lactate molecules bind covalently to lysine residues in proteins via ester bonds. The main regulatory factors of lactylation are typically associated with increased intracellular lactate concentrations. Furthermore, acylation-modifying enzymes, such as acyltransferase P300/CBP and delactase HDAC, play important roles. Previous studies have revealed that lactylation regulates the progression of numerous diseases, including tumors, sepsis and immune diseases (14,15). Recent research indicates that dexmedetomidine can regulate myocardial I/R-induced ferroptosis through MDH2 K241 lactylation (16). However, there are few studies on lactylation in MIRI, and the underlying mechanisms remain unexplored.

The present study aimed to investigate the mechanism and role of lactylation in MIRI regulation. It was observed that increased lactylation levels exacerbated mitochondrial and cardiac dysfunction following MIRI. Mechanistically, it was confirmed that IDH2 lactylation was upregulated after MIRI. This upregulation led to decreased enzymatic activity and α-KG-regulated AMPK phosphorylation. These findings improve understanding of the role of lactate in mitochondrial function and lay the groundwork for developing novel targeted therapies to improve MIRI.

Materials and methods

Animal experiment. The ethics approval (approval no. AHGDMU-LAC-B-202301-0004) for animal research was obtained from the Experimental Animal Ethics Committee of Guangdong Medical University (animal facility license, SYXK 2022-0286; Zhanjiang, China). C57BL/6 mice were purchased from SPF Biotechnology Co., Ltd. Mice were housed under SPF conditions in a controlled environment. The animal facility maintained a temperature of 22±2˚C and relative humidity of 50±10%, with a 12/12-h light/dark cycle (lights on at 7:00 a.m.). Ventilation was set at 15 air changes per hour, and all animals had *ad libitum* access to sterilized food and autoclaved water. All procedures complied with the institutional guidelines for animal care and use. A total of 110 male adult mice, weighing 25±5 g, were raised to 8-weeks old before receiving the experimental treatment. They were then fed normally for 1 week to reduce stress. A total of 100 neonatal mice were placed in a thermostatic incubator on postnatal day 2 to prepare for the isolation of primary cardiomyocytes.

I/R model. After successful intubation, the mice were connected with an anesthesia ventilator. Then, the intercostal space was fully expanded to expose the surgical field. An 8-0 suture needle was employed to ligate the threading of the left anterior descending coronary artery, and the left heart apex was white and the ECG showed MI. After 45 min of ischemia elapsed, the heart was re-exposed. The ligature was removed, and the ECG returned to normal, signifying successful reperfusion. Subsequently, the chest wall was sutured in layers, and resuscitation was carried out on a warming pad.

Anesthesia procedures. General anesthesia was achieved with isoflurane for all surgical interventions. Anesthesia was induced in an induction chamber with 5% isoflurane delivered in 100% oxygen at a flow rate of 1.5 l/min. Following the loss of righting and pedal reflexes, the mouse was secured in the supine position on a heated surgical platform equipped with continuous temperature maintenance. After orotracheal intubation, anesthesia was maintained by connecting the endotracheal tube to the gas delivery system, delivering 1.5-2.0% isoflurane in 100% oxygen at a constant flow rate of 0.9 l/min throughout the procedure.

Administration methods. Following myocardial I/R, mice were treated with either 400 mg/kg lactate (cat. no. L1750;

MilliporeSigma) via intraperitoneal (i.p.) injection, or with 50 mg/kg 3-(1H-1,2,3-Triazol-4-yl) pyridine (3-TYP; cat. no. HY-108331; MedChemExpress) i.p. 24 h prior to I/R. For genetic manipulation, 8-week-old mice received a tail vein (i.v.) injection of AAV9 virus ($2x10^{11}$ GC/mouse); surgical procedures were performed 14 days post-injection. Evans Blue-TTC staining: The areas of myocardial infarction and area at risk (AAR) after I/R were determined and evaluated using TTC (cat. no. T8877-5G; MilliporeSigma) and Evans blue stain (cat. no. E2129; MilliporeSigma) after 3 days of I/R modelling of mouse hearts. For the procedure, once the mice were anesthetized and intubated, a thin tube was inserted into the ascending aorta. Then, the aorta was perfused retrogradely with 1.5% Evans blue dye for 1 min. Subsequently, the entire heart was frozen for 10 min at -80˚C and sliced into 2 mm slices. After rewarming and setting, the slices were placed in 1.5% TTC solution and incubated at 37˚C for 10 min, followed by incubation in 10% formalin for 1 h. Finally, the slices were scanned, images were captured and analyzed.

Mouse echocardiography. Mice were depilated with a razor and anaesthetized with isoflurane. Mice were immobilized on a laboratory bench and cardiac function was assessed by echocardiography (Vevo 3100; Fujifilm Visual Sonics). The procedure was as follows: B-mode and M-mode images were acquired in parasternal short-axis views with an MS-400 ultrasound probe, and left ventricular end-systolic diameter, left ventricular end-diastolic diameter, left ventricular ejection fraction (LVEF%) and left ventricular fractional shortening (LVFS%) were examined and calculated for measurements in three consecutive cardiac cycles. EF% and FS% were calculated, and each group was replicated in 5 mice.

Animal euthanasia. According to the AVMA Guidelines for the Euthanasia of Animals (2020 Edition), at the end of the experimental protocol, all animals were humanely euthanized. Adult mice were deeply anesthetized with an i.p. injection of pentobarbital sodium (150 mg/kg body weight). Following confirmation of complete loss of pedal and righting reflexes, euthanasia was ensured by cervical dislocation prior to tissue collection. Neonatal mice were anesthetized with 2% isoflurane, and after confirming loss of consciousness and absence of reflexes, they were euthanized by cervical dislocation, followed by tissue collection (17).

Humane endpoints. Throughout the study, animals were monitored daily for signs of distress. The following humane endpoints were established: i) weight loss exceeding 20% of baseline body weight; ii) inability to ambulate or access food and water; iii) signs of severe respiratory distress; iv) persistent hypothermia; and v) moribund condition. Any animal meeting any of these criteria was immediately euthanized by cervical dislocation under deep isoflurane anesthesia to minimize suffering.

Cell culture and treatment

Primary cardiomyocytes. Briefly, ventricles from 2-day-old C57BL/6 neonatal mice (euthanized by cervical dislocation under 2% isoflurane anesthesia for 2 min) were excised, minced, and digested with 0.1% trypsin (cat. no. T1300; Beijing Solarbio Science & Technology Co., Ltd.) at 4˚C for 14 h, followed by two 15-min digestions with 0.1 mg/ml type II collagenase (cat. no. 9001-12-1; Beijing Solarbio Science & Technology Co., Ltd.) in PBS containing 5 mg/ml BSA at 37˚C under constant stirring. The cell suspension was collected, neutralized with two volumes of DMEM/10% fetal bovine serum (FBS; cat. no. 10099141C; Gibco; Thermo Fisher Scientific, Inc.) and centrifuged at 500 x g for 3 min. Cells were resuspended in DMEM supplemented with 10% FBS and 1% penicillin-streptomycin and plated onto 100-mm dishes for 2 h at 37˚C to allow fibroblast attachment (18,19). Non-adherent cardiomyocytes were collected, reseeded onto pre-coated dishes, and cultured at 37˚C in 5% CO_2.

Cell culture. Primary mouse cardiomyocytes and HL-1 cells (Cell Bank; Chinese Academy of Sciences) were cultured in high-glucose DMEM supplemented with 10% FBS at 37˚C in a 5% CO_2 humidified incubator.

Plasmids. Before transfection, 6-well plates were inoculated with $5x10^4$ cells/well in 3 ml of media and cultured for 24 h. When the cell confluence reached 40-50%, the cells were transfected with IDH2-WT and IDH2-K275R plasmid (2,000 ng/well) using lipofectamine 3000 reagent (cat. no. L3000015; Invitrogen; Thermo Fisher Scientific, Inc.) following the manufacturer's instructions (Table SI). After 8-10 h of incubation, cells' culture medium was replaced with normal medium, then these cells were used for further experiments.

Lentivirus transfection. ShRNAs (Table SII) were purchased from Shanghai Genechem Co., Ltd. Lentiviral particles were produced using a second-generation SIN packaging system. The three plasmids (GV-based transfer vector, pHelper1.0, and pHelper2.0) were co-transfected into 293T cells (Shanghai GeneChem Co., Ltd.). After a 6-h incubation at 37˚C, the medium was replaced. Viral supernatants were collected at 48 and 72 h post-transfection, pooled, and concentrated by ultracentrifugation (120,000 x g, 2 h, 4˚C) using a Beckman ultracentrifuge (Beckman Coulter, Inc.). The concentrated virus was resuspended in PBS and stored at -80˚C. The optimal multiplicity of infection (MOI) was predetermined as 100 in 96-well plates. For stable transfection, cells at 60% confluence were infected with LV-sh-IDH2 lentivirus ($5x10^5$ TU/ml) in infection solution P, followed by medium replacement at regular intervals. At 80-90% confluence, cells were expanded and selected with 3 μg/ml puromycin for 48 h. Stable clones were subsequently harvested and cryopreserved in liquid nitrogen or at -80˚C.

Hypoxia/reoxygenation (H/R) model. When the cell growth confluence was ~70-80%, the H/R model was established. The cells were washed twice with PBS. After that, an appropriate quantity of DMEM (without serum and antibiotics) was added. The parameters were preset in order to incubate the cells in a hypoxia incubator (37˚C, 95% N_2, 5% CO_2, 1% O_2) for 12 h. Complete culture medium was added, and the specimens were put into a regular constant temperature cell incubator for 3 h. These were then employed for the subsequent experiments.

Cell treatment. Experimental cells were pretreated with dichloroacetate (DCA; cat. no. B7174; APeXBIO Technology LLC) or sodium lactate (NaLac; cat. no. L7022; MilliporeSigma) for 24 h, both of the drug concentrations were 20 mmol/l. STO-609 (cat. no. S8274; Selleck Chemicals) was used at the concentration of 10 μmol/l for the inhibition of AMPK signaling pathway *in vitro*, which is a selective and cell-permeable inhibitor of CaM-KK2.

Lactate measurement. The lactate of blood, cell and myocardial tissue samples was measured using lactate assay kit (cat. no. BC2235; Beijing Solarbio Science & Technology Co., Ltd.). According to the instructions of the kit, the established standard curve was used to determine the OD value at the wavelength of 450 nm, and the lactate concentration was calculated accordingly.

Western blotting. Protein lysates were extracted from cardiac tissue and experimental cells. Protein concentrations were determined using the bicinchoninic acid (BCA) assay (cat. no. P0399S; Beyotime Institute of Biotechnology). Equal amounts of protein (30 μg per lane) were separated by electrophoresis on 10% SDS-polyacrylamide gels at 4˚C and subsequently transferred onto PVDF membranes at 4˚C. Following 1-h blocking with 5% non-fat milk at 25˚C, the membranes were incubated overnight with the following primary antibodies at 4˚C: phosphorylated (p-)AMPK (1:2,000; cat. no. 50081; Proteintech Group, Inc.), IDH2 (1:2,000; cat. no. D8E3B; Proteintech Group, Inc.), DRP1 (1:2,000; cat. no. 26187-1-AP; Proteintech Group, Inc.), MnSOD2 (1:2,000; cat. no. 66474-1-Ig; Proteintech Group, Inc.), AMPK (1:2,000; cat. no. 10929-2-AP; Cell Signaling Technology, Inc.), Cytochrome C (1:2,000; cat. no. PTM5351; PTM Biolab, Inc.; http://www.ptm-biolab.com.cn/index.html), Tubulin (1:4,000; cat. no. 11224-1-AP; Cell Signaling Technology, Inc.) and Pan-Kla (1:2,000; cat. no. PTM-1401; PTM Biolab, Inc.). Subsequently, the horseradish peroxidase-conjugated secondary antibody (1:5,000; cat. nos. SA00001-9 and SA00012-6; Proteintech Group, Inc.) was incubated for 1 h at ambient temperature. Visualization of the blots was achieved using enhanced chemiluminescence (ECL; cat. no. WBKLS0500 MilliporeSigma). Densitometric analysis was performed using ImageJ software (version 1.53t; National Institutes of Health).

Creatine kinase (CK)-MB. The CK-MB kit (cat. no. A032-1-1; Nanjing Jiancheng Bioengineering Institute) was used to reflect myocardial injury. After adding chromogen, the samples were incubated for 10 min at 37˚C. After washing, and absorbance values were measured at 450 nm.

Immunofluorescence staining. Cells or tissue sections were fixed with 4% paraformaldehyde for 15 min at room temperature, permeabilized with 0.1% Triton X-100 (cat. no. P0096; Beyotime Institute of Biotechnology) for 10 min and blocked with 5% BSA in PBS for 1 h at room temperature to reduce non-specific binding. Samples were then incubated overnight at 4˚C with the following primary antibodies: Pan-Kla (cat. no. PTM-1401; PTM Biolab, Inc.) and cTNT (cat. no. Ab005550; Beyotime Institute of Biotechnology) diluted 1:200 in blocking buffer. After washing three times with PBS, samples were incubated with the appropriate Alexa Fluor 488-conjugated goat anti-mouse IgG (H+L) (cat. no. A0428) and Alexa Fluor 594-conjugated goat anti-rabbit IgG (H+L) (cat. no. A0516; both from Beyotime Institute of Biotechnology) at a dilution of 1:500 for 1 h at room temperature in the dark. Nuclei were counterstained with DAPI (cat. no. 4083S; Cell Signaling Technology, Inc.; diluted to $5x10^{-4}$ mg/ml) for 5 min. Slides were mounted with antifade mounting medium and visualized using a fluorescence microscope (Olympus Corporation). Images were captured and processed using ImageJ software.

TUNEL staining. Apoptosis was assessed by TUNEL assay (cat. no. C1090; Beyotime Institute of Biotechnology). Fresh frozen myocardial sections (5 μm) were fixed with 4% paraformaldehyde (cat. no. P0099; Beyotime Institute of Biotechnology) for 30 min at room temperature, permeabilized with 0.1% Triton X-100 for 10 min, and incubated with TUNEL reaction solution for 2 h. After washing, sections were mounted and imaged by fluorescence microscopy (Olympus Corporation). At least five randomly selected fields of view per section were captured at x200 magnification for quantitative analysis.

ROS detection

DHE staining. Intracellular ROS levels were measured by DHE staining reagent (cat. no. S0063; Beyotime Institute of Biotechnology). The cells were incubated for 20 min at 37˚C in a serum-free medium supplemented with 10 μM DHE fluorescent probe. For animal experiments, 5-μm fresh-frozen slices of mouse hearts were prepared immediately after the experimental treatment; 100 μl of DHE working solution at a concentration of 20 μM was used for each slice, and the slices were incubated in a wet box and protected from light for 30 min at 37˚C. Fluorescence microscopy was utilized to examine and analyze the red fluorescence intensity of DHE.

MitoSOX staining. Mitochondrial ROS was determined by MitoSOX staining reagent (cat. no. MT14; Dojindo Laboratories, Inc.). Cells were added with the 10 μmol/l MitoSOX Deep Red working solution, and the sample was incubated for 30 min in a 5% CO_2 incubator at 37˚C. Following two washes with Hank's Balanced Salt Solution (cat. no. C0219; Beyotime Institute of Biotechnology), the fluorescence intensity was measured using a fluorescence microscope.

Mouse 8-OHdG production assay. The content of mouse 8-OHdG was determined by ELISA reagent (cat. no. E-EL-0028; Elabscience Biotechnology Co., Ltd.). The fresh cell homogenate was added to the microplate for detection according to the instructions of the manufacturer, and the OD value of the reaction products at 450 nm was detected by a microplate reader and calculated in accordance with the measured standard curve.

ATP measurement, mitochondrial membrane potential detection and NADPH/$NADP^+$ ratio assay. The ATP content was determined using an assay kit (cat. no. S0026; Beyotime Institute of Biotechnology) according to the manufacturer's instructions. Mitochondrial membrane potential was measured with a JC-1 kit (cat. no. C2003S; Beyotime Institute of Biotechnology). High levels of JC-1 monomers indicate a decrease in the mitochondrial membrane potential. After incubation according to the manufacturer's instructions, JC-1 monomers were measured using a BD FACSCanto II flow cytometer, and the data were analyzed with FlowJo software (version 10.8; BD Biosciences). The level of NADPH/$NADP^+$ was measured using a kit (cat. no. S0179; Beyotime Institute of Biotechnology).

Co-immunoprecipitation (Co-IP). Cells at 70-80% confluence were lysed in RIPA buffer at 4˚C for 20-30 min, and debris was removed by centrifugation (10,000 x g, 10 min, 4˚C). Supernatants containing 50-100 μg protein were incubated with primary antibody overnight at 4˚C, followed by incubation with 30 μl Protein A/G agarose beads for 4 h at 4˚C with gentle agitation. Beads were washed 3-5 times with PBS to remove no-specific binding, and bound proteins were eluted by boiling in SDS-PAGE loading buffer at 95˚C for 5-10 min. The eluate was collected by magnetic separation for subsequent analysis.

Transmission electron microscopy (TEM). Samples were fixed with 2.5% glutaraldehyde in 0.1 M phosphate buffer (pH 7.4) for 2 h at 4˚C, followed by post-fixation with 1% osmium tetroxide for 1 h at 4˚C, after dehydration, finally prepared as serial sections (80 nm) by an ultramicrotome and stained with uranyl acetate for 15 min at room temperature and lead citrate for 10 min at room temperature. After being rinsed and vacuum-dried at room temperature, the ultrastructure of the samples. Semi-quantitative analysis, using ImageJ software (version 1.53t; National Institutes of Health) to measure the size.

Oxygen consumption rate (OCR) assay. To measure the OCR, a 24-well XFe plate (Agilent Technologies, Inc.) was utilized. Cells were seeded at a density of $1x10^4$ per well and left to settle naturally for 1 h. Next, the cell plates were incubated overnight. Once the cell confluence reached 70-80%, the H/R model of cell culture was created. Thereafter, 0.5 μM rotenone, 1 μM FCCP and 2 μM oligomycin were added to each well according to the provided instructions. Subsequently, OCR was determined using a Seahorse XF analyzer.

IDH2 enzyme activity and α-KG content detection. An IDH activity assay kit (cat. no. S0526S; Beyotime Institute of Biotechnology) was used for enzyme activity detection. In accordance with the manufacturer's guidelines, fresh samples were diluted with buffer. These diluted samples were then incorporated into the NAD^+ reaction system, and the absorbance change at 450 nm was gauged using a microplate reader. A test kit (cat. no. ADS-F-S001; Jiangsu ADS Biotechnology Co., Ltd.) was used to detect α-KG, and the corresponding reagent and sample were added to the fresh sample supernatant after centrifugation (3,000 x g, 10 min, 4˚C). The mixture was vortexed evenly and then incubated at 37˚C in the dark for 10 min. The absorbance (OD) of each well at 450 nm wavelength was measured.

Omics sequencing and analysis

Proteomics. Heart tissue proteins were extracted, digested with trypsin, and lactylated peptides were enriched using anti-pan-Kla antibody beads. Enriched peptides were analyzed by liquid chromatography-mass spectrometry (LC-MS/MS) on a timsTOF Pro mass spectrometer (Bruker Daltonics; Bruker Corporation) operating in positive ionization mode with a capillary voltage of 1.60 kV. The instrument was operated in PASEF (parallel accumulation-serial fragmentation) mode. Precursors with charge states 0 to 5 were selected for fragmentation, and 10 PASEF-MS/MS scans were acquired per cycle with a dynamic exclusion of 30 s. Precursors and fragments were analyzed at the TOF detector over a mass range of 100-1,700 m/z. The nitrogen gas temperature was set to 180˚C, the nebulizer pressure to 1.4 bar, and the dry gas flow rate to 3.0 l/min. Raw data were searched against the UniProt mouse database using MaxQuant with FDR <1%. Bioinformatics analyzes included functional annotation [Gene Ontology, Kyoto Encyclopedia of Genes and Genomes (KEGG), subcellular localization], differential expression screening (fold change >1.5 or <0.67, P<0.05), enrichment analysis by Fisher's exact test, and protein-protein interaction network construction using STRING database (https://string-db.org/).

Metabolomics. Heart tissue metabolites were extracted and analyzed by UPLC-Q Exactive HF-X MS. Raw data were processed using Compound Discoverer 3.1 with metabolite identification against mzCloud and KEGG databases (https://www.kegg.jp/kegg/pathway.html). Metabolites with RSD >0.5 in QC samples were excluded. Missing values were imputed by KNN, followed by sum normalization and Pareto scaling. OPLS-DA was performed to identify differential metabolites (VIP >1, fold change >1.5 or <0.67, P<0.05). Pathway enrichment was conducted using KEGG with Fisher's exact test (P<0.05).

Molecular docking. PDB structure files of IDH2 were downloaded from the UniProt database (https://www.uniprot.org/), and SDF structure files of isocitrate were obtained from the PubChem database (https://pubchem.ncbi.nlm.nih.gov/). GROMACS software (version 2020.4; GROMACS development team; https://www.gromacs.org) was used to simulate the molecular dynamics of the modified IDH2 protein structure. PyMOL 2.1 software (version 2.1; Schrödinger, LLC; https://pymol.org) was used to visualize the spatial conformation of the amino acid side chain of the simulated IDH2 K275la (Tables SIII and SIV).

Quantification and statistical analyses. All quantitative data were obtained from independent experiments with triplicate repeats, and expressed as the mean ± SD. Two-tailed unpaired Student's t-test between two groups and one-way ANOVA followed by Bonferroni test for multiple comparison were performed for statistical analysis using SPSS 15.0 software (SPSS, Inc.). P<0.05 was considered to indicate a statistically significant difference.

Results

Elevated lactate and lactylation levels are associated with MIRI. To investigate the changes in lactate and lactylation during MIRI, a mouse model of MIRI was developed. Lactate levels were significantly elevated in both peripheral blood and myocardial tissue (Fig. 1A), with myocardium experiencing a peak at 6 h post-I/R, followed by a gradual decline (Fig. S1A). Quantification using pan-antibody staining confirmed a significant increase in lactate levels in the myocardial tissue (Fig. 1B and C).

Subsequently, exogenous lactate was administered to assess its effects on MIRI. The introduction of exogenous lactate increased myocardial lactate accumulation compared with the

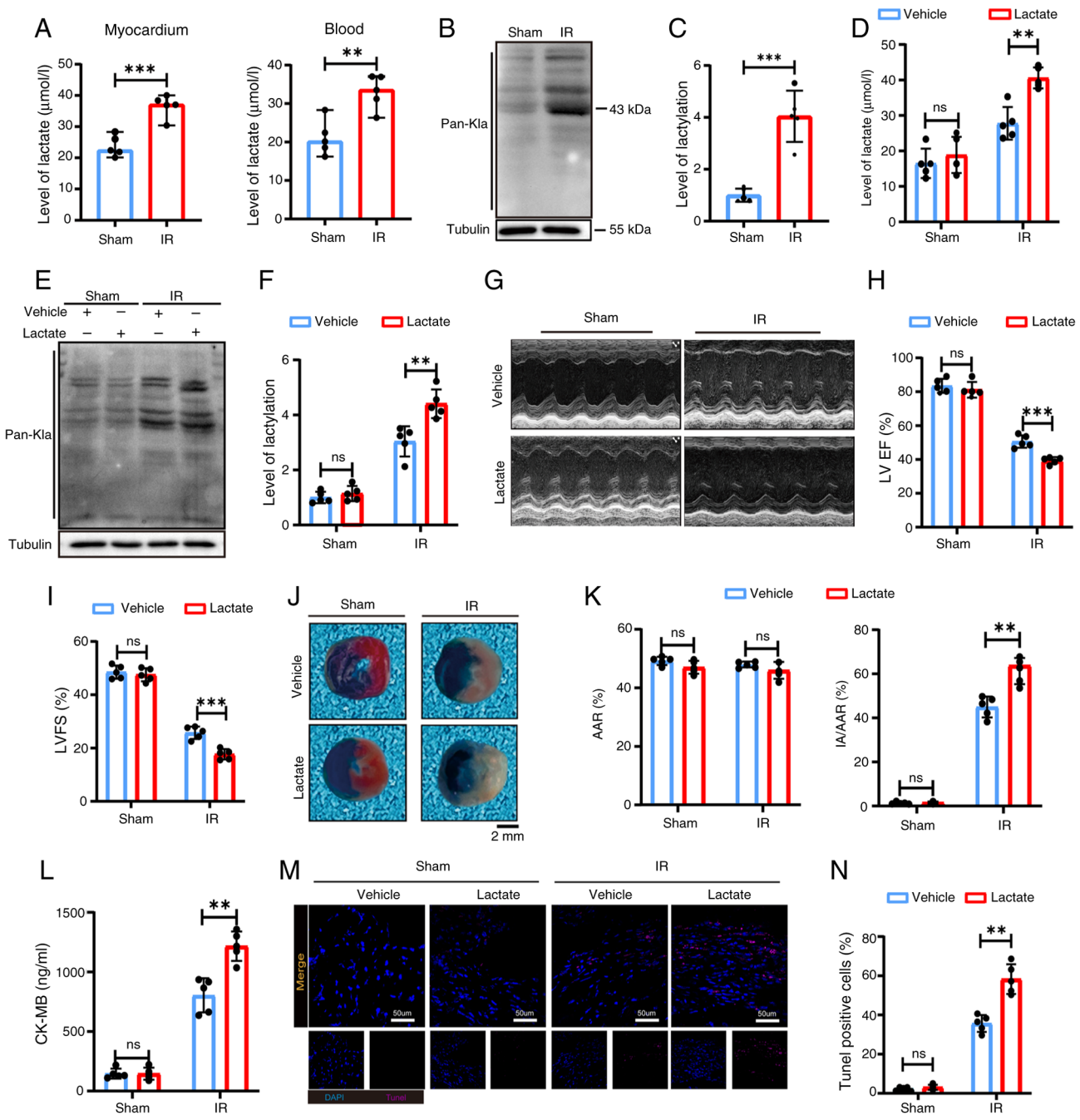

Figure 1. Elevated lactate and lactylation levels are associated with myocardial ischemia-reperfusion injury. (A) The concentration of lactate in myocardial tissue and blood of mice determined by a lactate detection kit (n=5). (B and C) Western blot for total level of lactylation in mouse myocardial tissue and its semi-quantitative analysis (n=5). (D) The determination of lactate in myocardial tissue after exogenous lactate administration (n=5). (E and F) The total level of lactylation in myocardium detected by western blot and its semi-quantitative analysis (n=5). (G-I) Echocardiography to evaluate cardiac function and quantitative analysis of LVEF% and LVFS% (n=5). (J and K) Evans blue-TTC staining for determining the ischemic area of myocardial injury and quantitative analysis of AAR% and IA/AAR% (n=3, scale=2 mm); (L) The level of CK-MB in myocardium detected by a CK-MB assay kit (n=5). (M and N) The positive rate of myocardial apoptosis detected by TUNEL staining (n=5). These data were representative results of three repetitions at least. Data are expressed as the mean ± SD. **P<0.01 and ***P<0.001. LVEF, left ventricular ejection fraction; LVFS, left ventricular fractional shortening; AAR, area at risk; IA, myocardial infarction; CK, creatine kinase; I/R, ischemia/reperfusion; ns, not significant.

I/R group (Fig. 1D), along with a significant upregulation of lactylation (Fig. 1E and F). The I/R + lactate group exhibited a significant decline in cardiac function and increased injury compared with the I/R + vehicle group. These results were demonstrated by decreases in LVFS% and LVEF% (Fig. 1G-I) and increased myocardial infarct size (Fig. 1J and K).

Furthermore, exogenous lactate administration led to higher CK-MB levels (Fig. 1L) and increased cardiomyocyte apoptosis, as indicated by TUNEL staining (Fig. 1M and N) compared with the I/R group. These findings suggest that lactylation levels are elevated in MIRI, which may contribute to enhanced myocardial injury and adverse outcomes.

Myocardial mitochondrial dysfunction is affected by lactylation in vitro. To further investigate the effect of lactylation on MIRI, HL-1 cells and primary cardiomyocytes

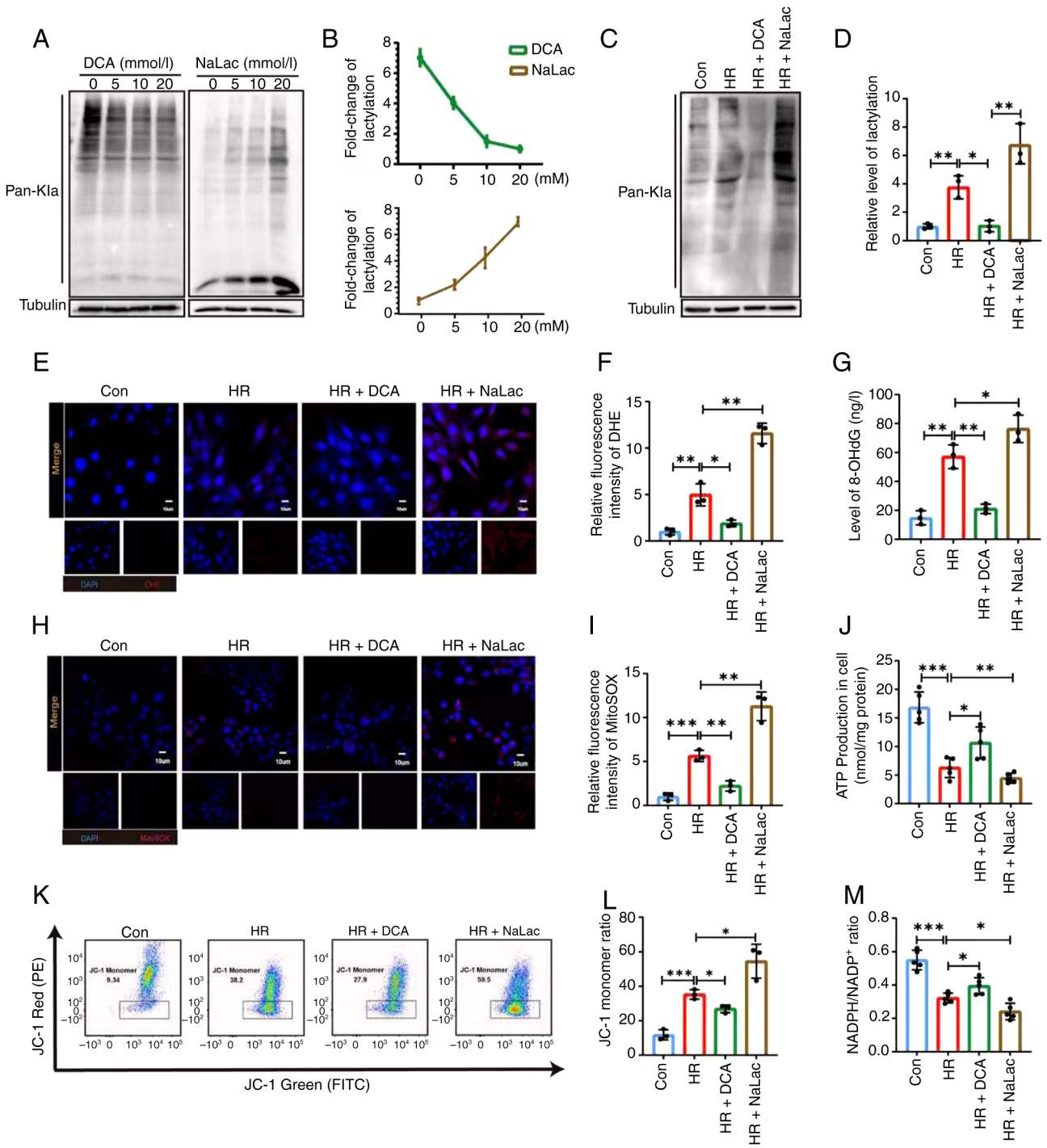

Figure 2. Myocardial mitochondrial dysfunction is affected by lactylation *in vitro*. (A and B) Western blot for the total level of lactylation in HL-1 cells treated with DCA and NaLac concentration gradient at 0, 5, 10, 20 mM and its semi-quantitative analysis (n=3). (C and D) The level of lactylation under HR in primary cardiomyocytes detected by western blotting and quantitative analysis (n=3). (E and F) The level of ROS in cardiomyocytes detected by DHE staining and quantitative analysis (n=3). (G) Determination of 8-OHdG in cardiomyocytes (n=3). (H and I) Mitochondrial ROS level detected by MitoSOX staining and quantitative analysis (n=3). (J) Measurement of intracellular ATP production (n=5). (K and L) The changes of mitochondrial membrane potential in cardiomyocytes detected by JC-1 flow cytometry (n=3). (M) The measurement of intracellular NADPH/NADP$^+$ levels (n=5). These data were representative results of three repetitions at least. Data are expressed as the mean ± SD. *P<0.05, **P<0.01 and ***P<0.001. DCA, dichloroacetate; NaLac, sodium lactate; H/R, hypoxia/reoxygenation; ROS, reactive oxygen species; 8-OHdG, 8-hydroxy-2'-deoxyguanosine.

were pretreated with NaLac or DCA, a lactate dehydrogenase inhibitor, as aforementioned. A dose-dependent reduction in cell lactylation was observed following treatment with varying concentrations of DCA. Conversely, cells treated with NaLac exhibited a gradient increase in lactylation (Fig. 2A and B). Pan-modified antibody detection indicated that lactylation levels were higher in the H/R group than in the Control (Con) group. However, DCA administration decreased lactylation levels compared with the HR group, and NaLac treatment further increased them (Fig. 2C and D). Immunofluorescence staining revealed similar trends in and Pan-Kla levels (Fig. S1B and C).

Given the established link between cellular lactate levels and mitochondrial dysfunction in disease, it was investigated whether lactylation is involved in H/R-induced mitochondrial dysfunction in cardiomyocytes. First, DHE and MitoSOX staining demonstrated that inhibiting lactate production decreased H/R-induced mitochondrial ROS production in cardiomyocytes, whereas the addition of exogenous NaLac further promoted intracellular ROS production (Fig. 2E, F, H and I). Similarly, H/R increased the mitochondrial damage marker 8-OHdG (Fig. 2G), reduced ATP production (Fig. 2J), decreased mitochondrial membrane potential (Fig. 2K-M), and lowered NADPH levels. These manifestations of mitochondrial dysfunction were further aggravated by NaLac treatment compared with the HR group. However, the addition of DCA ameliorated the H/R-induced mitochondrial dysfunction phenotypes. Collectively, these findings indicate that myocardial mitochondrial dysfunction is affected by lactylation *in vitro*.

IDH2 K275 lactylation levels are elevated in I/R myocardium. The lactylome proteomics analysis was performed to identify specific lactylation targets in myocardial I/R (Fig. 3A). LC-MS analysis revealed that 98 proteins exhibited decreased lactylation and 16 exhibited increased lactylation in the I/R group compared with the sham-operated group. Furthermore, 144 sites exhibited reduced lactylation and 19 exhibited increased lactylation (Fig. 3B). Functional analysis of the lactylated proteins revealed predominant mitochondrial localization (Fig. 3C). An enrichment analysis of the genes associated with increased levels of lactylation revealed entries related to the oxidoreduction coenzyme metabolic process and upregulation of the redox homeostasis biological process (Fig. 3D).

Based on the top 20 altered sites (Fig. 3E), a protein-protein interaction network constructed using the STRING database identified IDH2 as a key hub protein (Fig. 3F). Collision-induced dissociation analysis demonstrated a characteristic tandem MS spectrum at the lysine (K) site of IDH2 (Fig. 3G). Genetic conservation analysis of the IDH2 lysine sites across multiple species using the UniProt website revealed that the IDH2 K275 site was conserved across species (Fig. 3H). IDH2 is an important rate-limiting enzyme in the tricarboxylic acid (TCA) cycle. It catalyzes the oxidative decarboxylation of isocitrate to provide energy and support metabolic processes. The results of non-targeted metabolomics also indicated a decrease in the concentration of its catalytic product, α-KG (Fig. S2A). Animal and cellular I/R models exhibited significantly elevated IDH2 lactylation in Co-IP assays (Figs. 3I and S2B). This lactylation was pharmacologically modulated: DCA decreased it, and NaLac increased it in a concentration-dependent manner, without affecting total IDH2 expression (Figs. 3J and S2C). Lactylome analysis indicated elevated lactylation at K256 and K275. Therefore, the deacylating mutant plasmids K256R and K275R were used to identify the major lactylation sites in IDH2. Co-IP assay revealed a more significant reduction in lactylation in K275R than in K256R (Figs. 3K and S2D), suggesting that K275 plays a predominant role in IDH2 lactylation. Therefore, it is proposed that the primary factor contributing to the impairment of protein function and enzyme activity in MIRI is the lactylation of IDH2, rather than changes in its protein expression. This, in turn, affects a series of downstream mitochondrial functions. These findings indicate that IDH2 K275 may be a key regulatory site for MIRI.

K275 mutant effectively attenuates mitochondrial dysfunction in H/R cardiomyocytes. HL-1 cell lines with stable IDH2 knockout were established using lentivirus to investigate whether IDH2 K275la affects mitochondrial homeostasis (Fig. S3A and B) and subsequently transfected with an IDH2 K275 mutant plasmid for rescue experiments. Co-IP results indicated that the K275R mutant group in the H/R model exhibited no IDH2 lactylation compared with the wild-type (WT) group (Fig. 4A and B). In the HR group, ATP content and the NADPH/$NADP^+$ ratio decreased, whereas 8-OHdG levels increased. However, the markers associated with mitochondrial function were significantly improved in the K275 mutant group (Fig. 4C-E). The OCR assay results revealed impaired maximum mitochondrial levels and basal respiratory rates in the HR-WT group compared with the Con group. However, these findings were reversed in the K275 mutation (Fig. 4F and G). DHE and MitoSOX fluorescence staining indicated that mitochondrial ROS levels were significantly higher in the HR + WT group than in the Con group. Conversely, the K275 mutant decreased mitochondrial ROS production (Fig. 4H-K). The mutant group consistently stabilized the H/R-induced loss of mitochondrial membrane potential, as indicated by an increased JC-1 monomer ratio (Fig. 4L and M). Western blots confirmed the reversals in the effects on mitochondrial dynamin DRP1, MnSOD2, and mitochondrial apoptosis Cytochrome C (Cyt C) in the HR-WT treated group with a K275 mutant plasmid (Fig. 4N and O). These findings indicate that lactylation at the K275 site of IDH2 is essential in regulating H/R-induced mitochondrial dysfunction in cardiomyocytes.

IDH2 K275la reduces IDH2 activity and exacerbates mitochondrial dysfunction in cardiomyocytes by inhibiting the phosphorylation of AMPK. It was previously reported that IDH2 product α-KG activates AMPK via upstream kinases (20). It was hypothesized that IDH2-α-KG-AMPK axis regulates mitochondrial function (Fig. 5A). IDH2 catalytic activity was examined at varying NaLac concentrations. IDH2 enzymatic activity was inversely correlated with NaLac concentration (Fig. 5B). Correspondingly, α-KG levels also decreased with increases in NaLac concentration. This downward trend was consistent with that of IDH2 (Fig. 5C). Subsequently, it was observed that IDH2 catalytic activity and α-KG content decreased in the HR-WT group compared with the Con group and reversed by IDH2 K275R (Fig. 5D and E).

Molecular dynamics simulations of the modified IDH2 protein structure were performed using GROMACS to clarify the specific molecular structural changes upon lactylated IDH2 binding to isocitric acid. The average docking binding energy scores of IDH2 with its substrate increased after lactylation. The binding affinity of the modified IDH2 and isocitric acid was reduced according to the principle of the lowest binding energy and the highest binding affinity. Furthermore, visualization of the IDH2 tertiary structure following lactylation revealed that IDH2 K275la may affect local stability. This was accomplished by impeding the formation of the salt

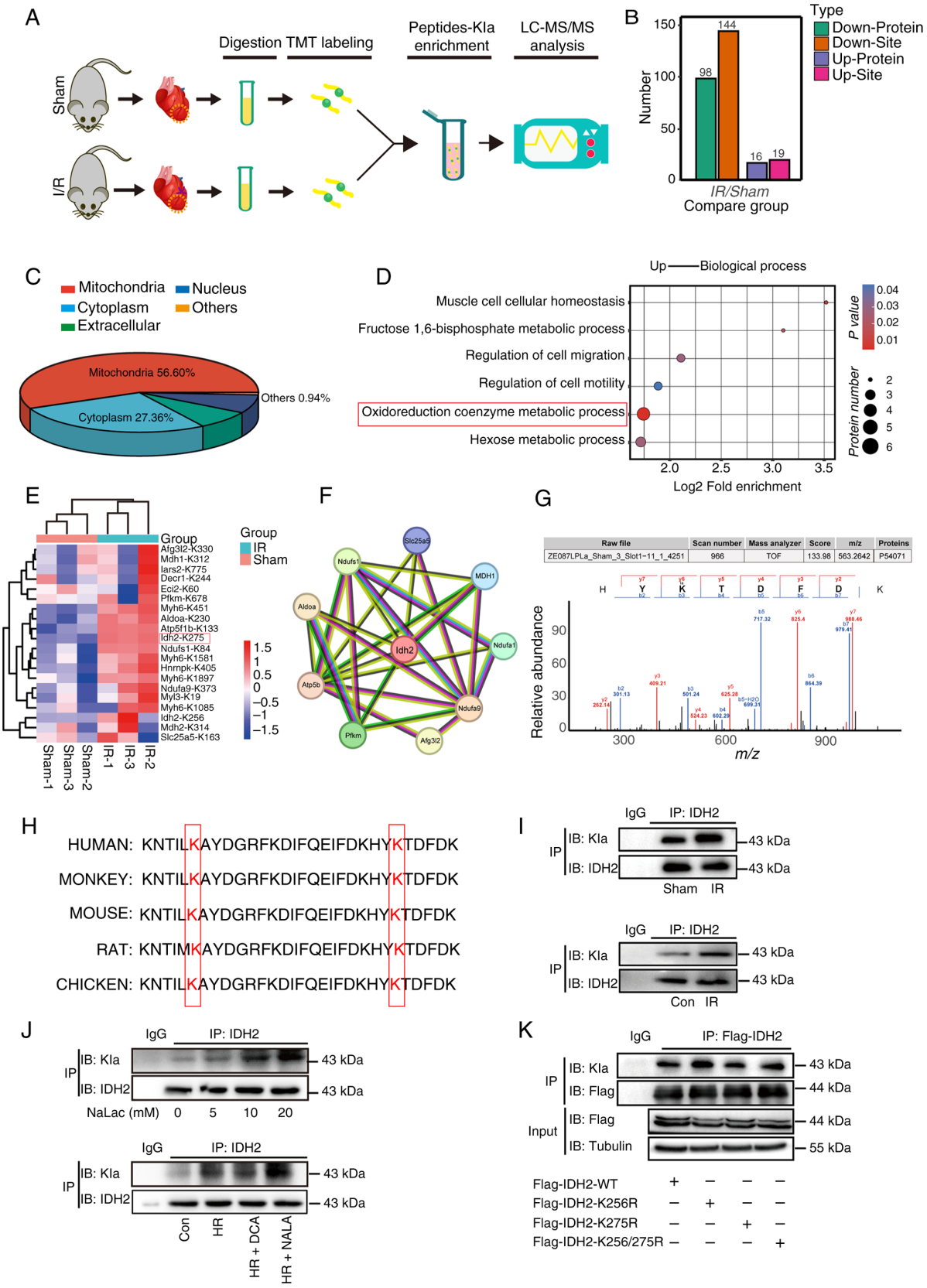

Figure 3. Level of IDH2 K275 lactylation is elevated in ischemia-reperfusion myocardium. (A) Schematic diagram of the analysis process of lactylomics. (B) DELPs identified by comparing I/R and sham groups (Sham group, n=9; IR group, n=9). (C) Subcellular localization of DELPS. (D) Gene functional enrichment analysis. (E) Heat map shows top 20 lactylation protein and site. (F) Protein-protein interaction network diagram of mitochondria-associated lactylation proteins. (G) The lysine site of IDH2 characteristic tandem. (H) Genetic conservation of IDH2 lysine sites across species. (I) IDH2 lactylation in animal (n=5) and primary cardiomyocytes (n=3) detected by IP experiment. (J) The level of IDH2 lactylation after treating with NaLac and DCA detected by IP experiments (n=3). (K) IDH2 lactylation levels after transfection of the IDH2 K256 mutant plasmid and the IDH2 K275 mutant plasmid detected by IP experiment (n=3). These data were representative results of three repetitions at least. Data are expressed as the mean ± SD. IDH2, isocitrate dehydrogenase 2; DELPs, differentially expressed lactylation proteins; I/R, ischemia/reperfusion; IP, immunoprecipitation; DCA, dichloroacetate; NaLac, sodium lactate; WT, wild-type.

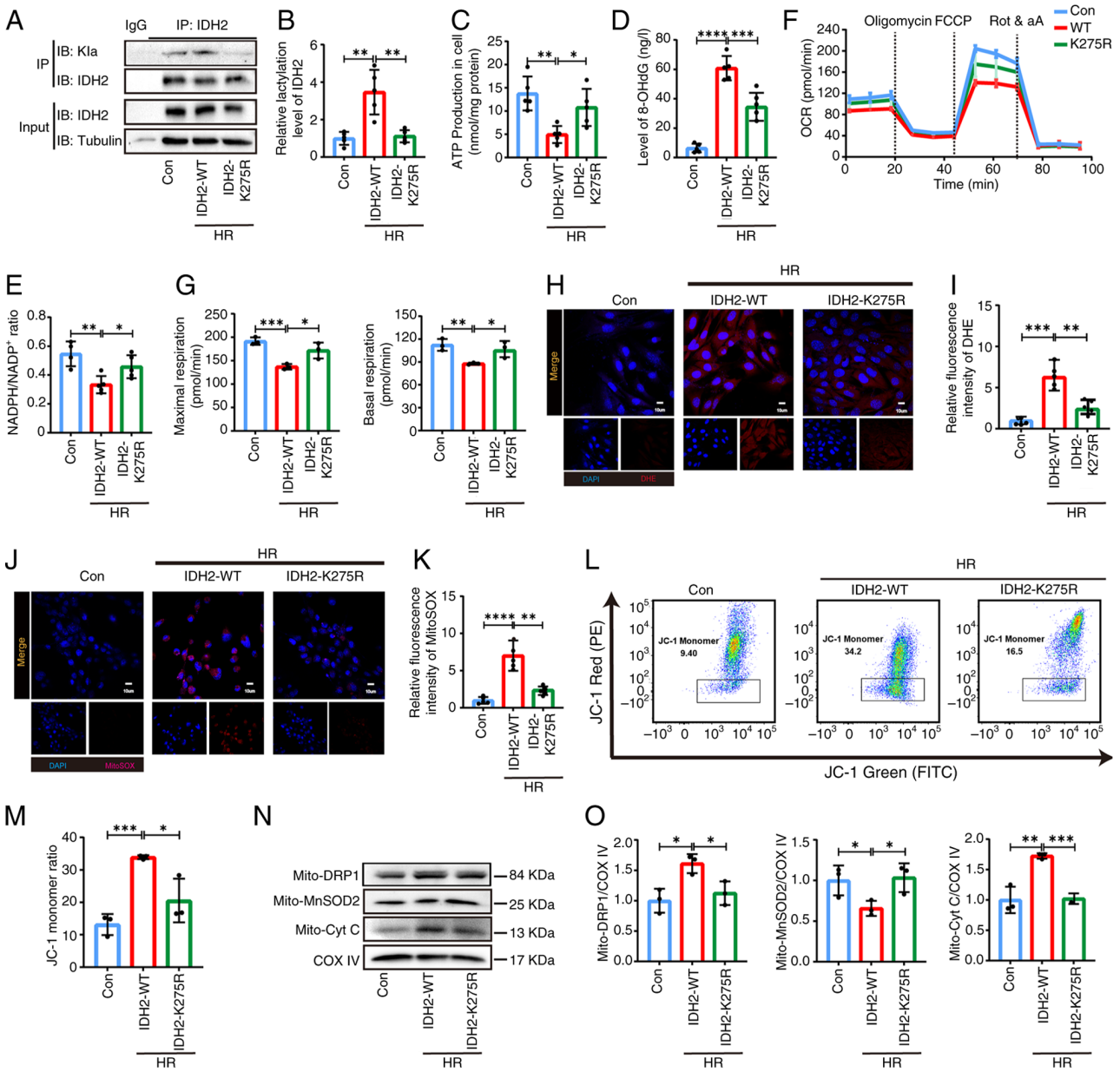

Figure 4. K275 mutant effectively attenuates mitochondrial dysfunction in H/R cardiomyocytes. (A and B) IP experiment for the lactylation level of IDH2 in IDH2-WT and IDH2 K275R plasmids and quantitative analysis (n=5). (C) Detection of intracellular ATP production after plasmid transfection (n=5). (D) 8-OHdG levels in cardiomyocytes (n=5). (E) Intracellular NADPH/NADP+ levels (n=5). (F and G) Oxygen consumption rate measured by mitochondrial stress test in HL-1 cells and quantitative respiration function (n=3). (H and I) DHE staining assay for reactive oxygen species level in cells and quantitative analysis (n=5). (J and K) The mitochondrial oxidative stress level of cardiomyocytes detected by MitoSOX staining (n=5). (L and M) Mitochondrial membrane potential in HL-1 cardiomyocytes detected by JC-1 staining flow cytometry and quantitative analysis (n=3). (N and O) The protein levels of DRP1, MnSOD2 and Cyt C protein expression detected by western blot (n=3). These data were representative results of three repetitions at least. Data are expressed as the mean ± SD *P<0.05, **P<0.01 and ***P<0.001. H/R, hypoxia/reoxygenation; IDH2, isocitrate dehydrogenase 2; WT, wild-type; IP, immunoprecipitation; 8-OHdG, 8-hydroxy-2'-deoxyguanosine; DRP1, dynamin-related protein 1; MnSOD2, manganese superoxide dismutase 2; Cyt C, cytochrome C.

bridge between Lys275 and ASP279 in the protein structure. Consequently, the spatial conformation of the amino acid side chain was readily altered, preventing IDH2 from binding to its substrate and thereby reducing its catalytic activity (Fig. 5F).

The AMPK phosphorylation inhibitor, STO-609, was used to determine whether this pathway mediates K275la effects. Western blot analysis demonstrated that the K275 mutation increased p-AMPK levels, along with beneficial changes in MnSOD2, DRP1 and Cyt C. As expected, STO-609 treatment abolished the increased AMPK phosphorylation and the mitochondrial protective effects of the K275 mutation (Fig. 5G-K). However, mitochondrial ROS production was significantly increased after STO-609 treatment compared with the HR + IDH2 + K275R group (Fig. 5L and M).

Furthermore, cells were exposed to α-KG to validate its mediation of mitochondrial dysfunction. Western blot analysis revealed that α-KG treatment in the H/R model restored AMPK phosphorylation levels compared with the HR group. Treatment of myocytes with α-KG reduced the expression of the mitochondrial kinetic protein DRP1 and increased the levels of the antioxidant protein MnSOD2 (Fig. S3C and D). These results indicate that IDH2 K275la downregulates IDH2

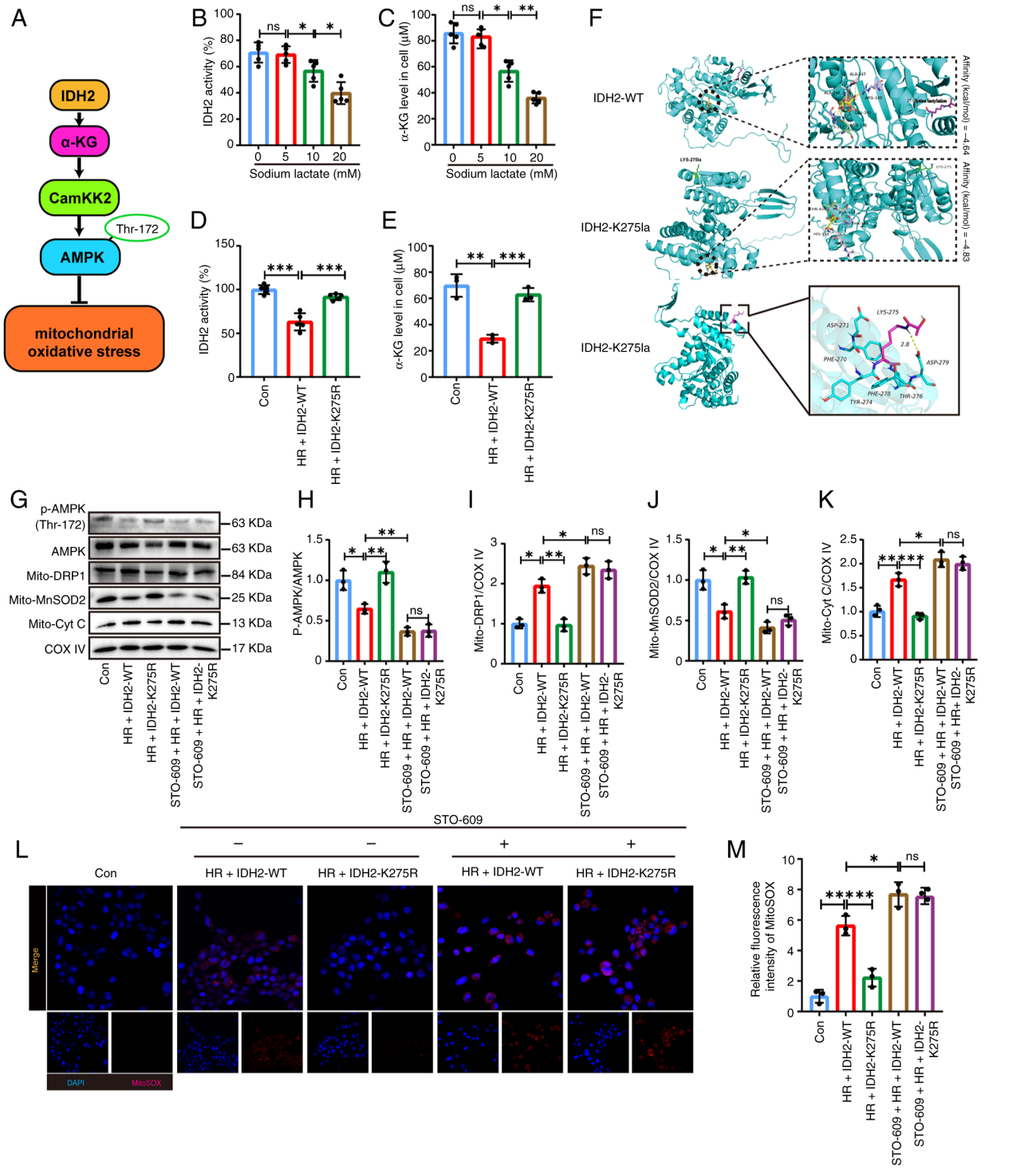

Figure 5. IDH2 K275la reduces IDH2 activity and exacerbates mitochondrial dysfunction in cardiomyocytes by inhibiting the phosphorylation of AMPK. (A) The mechanism diagram of the conjecture. (B) Detection of IDH2 activity under 0, 5, 10, 20 mM sodium lactate gradient (n=5). (C) Detection of α-KG production under sodium lactate gradient (n=5). (D) Detection of IDH2 activity by comparing between WT and K275R mutant (n=5). (E) α-KG production between WT and K275R mutant detected by α-KG assay kit (n=3). (F) Molecular dynamics simulation of IDH2 structure before and after lactylation using GROMACS software, and visualization of the lactylated IDH2 tertiary structure using PyMOL 2.1. (G-K) Protein levels of p-AMPK, AMPK, DRP1, MnSOD2 and Cyt C detected by western blotting after STO-609 treatment, and their semi-quantitative analyzes (n=3). (L and M) Representative images of MitoSOX staining for STO-609 treatment group (n=3). These data were representative results of three repetitions at least. Data are expressed as the mean ± SD. *P<0.05, **P<0.01 and ***P<0.001. IDH2, isocitrate dehydrogenase 2; AMPK, adenosine 5'-monophosphate-activated protein kinase; α-KG, α-ketoglutaric acid; WT, wild-type; p-, phosphorylated; DRP1, dynamin-related protein 1; MnSOD2, manganese superoxide dismutase 2; Cyt C, cytochrome C; H/R, hypoxia/reoxygenation; ns, not significant.

catalytic activity and exacerbates mitochondrial dysfunction in cardiomyocytes by inhibiting the phosphorylation-activation of the α-KG/AMPK pathway.

Inhibition of IDH2 K275la alleviates MIRI and partially eliminates the aggravating effect of lactate on cardiac tissue. To validate the *in vivo* role of IDH2 K275, mice were administered

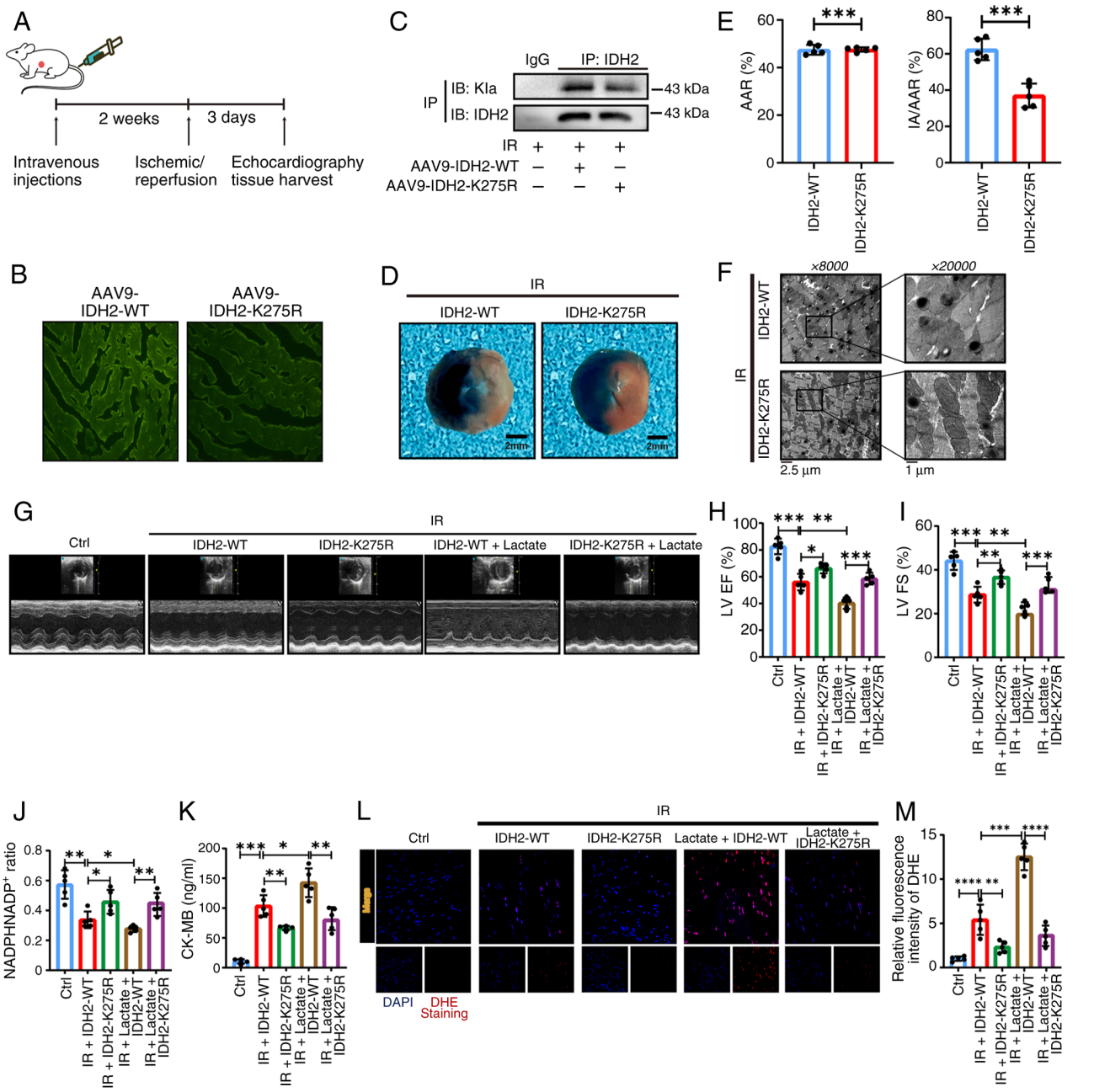

Figure 6. Inhibition of IDH2 K275la alleviates myocardial ischemia-reperfusion injury and partially eliminates the aggravating effect of lactate on cardiac injury. (A) Schematic diagram of virus injection method and experimental scheme. (B) The efficiency of virus infection in mouse heart observed by fluorescence microscopy (n=5). (C) IP assay for detecting the IDH2 lactylation after cardiac virus infection (n=5). (D and E) Evans blue-TTC staining showing ischemic area of myocardial infarction (scale, 2 mm; n=5). (F) Electron microscopy of mitochondria in mouse left ventricular myocardium (scale, 1 μm; n=5). (G-I) Echocardiography to evaluate cardiac function and quantitative analysis of LVEF% and LVFS% (n=5). (J) NADPH/NADP$^+$ ratio in mouse myocardial tissue (n=5). (K) CK-MB content in myocardial tissue of mice (n=5). (L and M) The reactive oxygen species production level detected by DHE staining (n=5). These data were representative results of three repetitions at least. Data are expressed as the mean ± SD. *P<0.05, **P<0.01 and ***P<0.001. IDH2, isocitrate dehydrogenase 2; IP, immunoprecipitation; LVEF, left ventricular ejection fraction; LVFS, left ventricular fractional shortening; CK, creatine kinase; WT, wild-type; I/R, ischemia/reperfusion; IA, myocardial infarction; AAR, area at risk.

AAV9 carrying IDH2-WT or IDH2-K275R via the tail vein 14 days before I/R surgery (Fig. 6A). A green fluorescent protein (GFP) tag demonstrated successful infection with GFP-tagged viruses (Fig. 6B), and Co-IP experiments confirmed that the virus reduced IDH2 lactylation in the myocardium compared with the WT group (Fig. 6C). Subsequently, Evans blue-TTC staining revealed a smaller myocardial infarct area in K275R mice (Fig. 6D and E). TEM revealed a large number of irregularly accumulated heart mitochondria, swollen mitochondria, and destroyed mitochondrial ridge structures, while mitochondrial swelling improved, the structure recovered, and the arrangement became regular in the mutant group (Fig. 6F). The K275 mutant group demonstrated improved cardiac function (LVEF% and LVFS%), increased NADPH/NADP$^+$ ratio, and decreased markers of myocardial damage and ROS production compared with the I/R group. Notably, the exacerbation of these parameters by exogenous NaLac was partially reversed in the K275R mice (Fig. 6G-M). These results suggest

that inhibiting IDH2-K275la alleviated MIRI and partially eliminated the disease-aggravating effect of lactate on cardiac tissue.

SIRT3 regulates myocardial oxidative injury by delactylating IDH2 in MIRI. Lactylation is a newly identified form of acylation modification that may share comparable regulatory enzymes with other lysine acylation modifications. It has been recently suggested that Sirtuins (SIRTs) may regulate lactylation (21). RCSB and UniProt databases were used to analyze the molecular docking of several known acylation-modifying SIRT enzymes with IDH2 and to explore the regulatory enzymes that affect IDH2 lactylation. SIRT3, 4, and 6 exhibited strong binding affinity for IDH2 (Fig. 7A). Co-IP identified SIRT3 as the most potent inhibitor of IDH2 lactylation, whose expression was decreased in the I/R model (Fig. 7B and C). Previous studies have demonstrated that SIRT3 levels are reduced in I/R injury, and that SIRT3 overexpression promotes recovery of cardiac function and reduces injury markers in reperfusion injury (22). 3-TYP, a specific SIRT3 inhibitor, was used to investigate whether SIRT3 regulates IDH2 lactylation *in vivo*. The findings of the present study revealed that 3-TYP did not affect the SIRT3 expression. Rather, it inhibited the delactylation function of SIRT3 and increased IDH2 lactylation. Conversely, the effect of 3-TYP was nullified in mice treated with the K275 mutant (Fig. 7D and E). 3-TYP treatment downregulated α-KG content compared with the WT group, an effect reversed in the K275 mutation group (Fig. 7F). 3-TYP administration further reduced AMPK phosphorylation, increased the expression of mitochondrial function-related proteins DRP1 and Cyt C, decreased MnSOD2, downregulated the proportion of reduced coenzyme, elevated ROS production, and increased CK-MB compared with the I/R + WT group. Conversely, the IDH2 mutant reversed the previously described inhibition of AMPK phosphorylation and mitochondrial dysfunction and increased the 3-TYP-induced damage markers (Fig. 7G-K). These findings indicate that SIRT3 is the upstream regulatory enzyme of IDH2 acylation and that IDH2 K275 is a critical regulatory site for SIRT3-mediated myocardial injury in MIRI.

Discussion

The present study demonstrated that hyper-lactylation, triggered by increased lactate levels, contributes to the early aggravation of I/R injury in mice. The findings of the present study reveal that IDH2 K275 lactylation impairs its catalytic activity, reduces α-KG production, and alters activation of the AMPK signaling pathway, thereby leading to mitochondrial dysfunction. The present study is the first, to the best of our knowledge, to demonstrate that IDH2 can be modified by lactylation in addition to acetylation and identifies K275 as a novel functional site in I/R hearts. Furthermore, by exploring the relationship between lactylation and mitochondrial function, it was identified, for the first time, that IDH2 lactylation can regulate its activity, thereby affecting mitochondrial function. These findings advance the understanding of the physiological role of lactylation, provide a novel perspective on MIRI pathogenesis, and suggest potential therapeutic strategies.

Lactate, previously considered a metabolic waste product, is now recognized as essential for cellular functions. For instance, lactate can be transported to cells, absorbed, used, oxidized, and metabolized in the mitochondria to provide energy for cells (23), indicating that lactate can be used as a metabolic fuel in emergencies. Furthermore, lactate can eliminate and suppress immune cells in the immune microenvironment (24). In 2019, lactate was found to exert its function through histone lactylation, providing new insights into its role. Subsequent research has demonstrated that lactylation is prevalent among non-histone proteins across various cell types and plays significant roles in energy metabolism, cell signaling, transcriptional regulation and organ dysfunction (25,26). For instance, lactylation plays a key regulatory role by activating the ubiquitin-proteasome system, leading to the retention of erythrocyte mitochondria and contributing to lupus (27). Furthermore, in cardiovascular disease, the downregulation of α-MHC lactylation may result in structural and functional impairments of the heart and exacerbate heart failure (28). Regarding immune regulation, PKM2 lactylation suppresses the inflammatory metabolic adaptation of pro-inflammatory macrophages (29). The present findings are consistent with this expanding understanding. A lactate-concentration-dependent increase in lactylation was observed in the I/R model, and lactate supplementation exacerbated myocardial dysfunction. DCA ameliorated H/R-induced mitochondrial dysfunction *in vitro*, whereas NaLac exacerbated this effect. However, the mechanism by which lactate contributes to the occurrence and progression of I/R myocardial injury remains unclear and warrants further study.

IDH2, a mitochondrial isoform of isocitrate dehydrogenase, is a key enzyme in the TCA cycle. It contributes to energy production and cellular redox balance by catalyzing the oxidative decarboxylation of isocitrate to α-KG and producing NADPH (30,32). IDH2 helps defend against oxidative stress by maintaining cellular NADPH pools (31). Its dysfunction, associated with elevated ROS and mitochondrial impairment, is implicated in cancer, neurodegenerative diseases and aging (33-35). For instance, IDH2 deficiency in mice exacerbates mitochondrial oxidative stress in the liver and accelerates age-associated phenotypes (36). In cardiac pathology, IDH2-null mice are more susceptible to pressure overload-induced hypertrophy, leading to cardiomyocyte metabolic dysregulation and oxidative stress (37). Notably, the oncometabolite 2-HG is produced by gain-of-function mutations in IDH2 (for instance, R172), which drive oncogenesis in AML and gliomas (38). This has rendered mutant IDH2 a promising therapeutic target, with inhibitors such as enasidenib and vorasidenib developed for clinical use (39,40). Targeting protein sites with drugs disrupts cellular metabolism and inhibits tumor cell proliferation. This suggests that the precise targeting of key protein modification sites is effective for disease treatment. In the present study, IDH2 K275 was mutated in cells to reduce lactylation. This mutation improved mitochondrial function in cardiomyocytes. Furthermore, the present study demonstrated that IDH2 mutation can alleviate I/R-induced heart injury in animal experiments. These findings provide a practical approach for treating MIRI and may represent a novel therapeutic target. However, further investigation is required to determine the factors regulating lactylation.

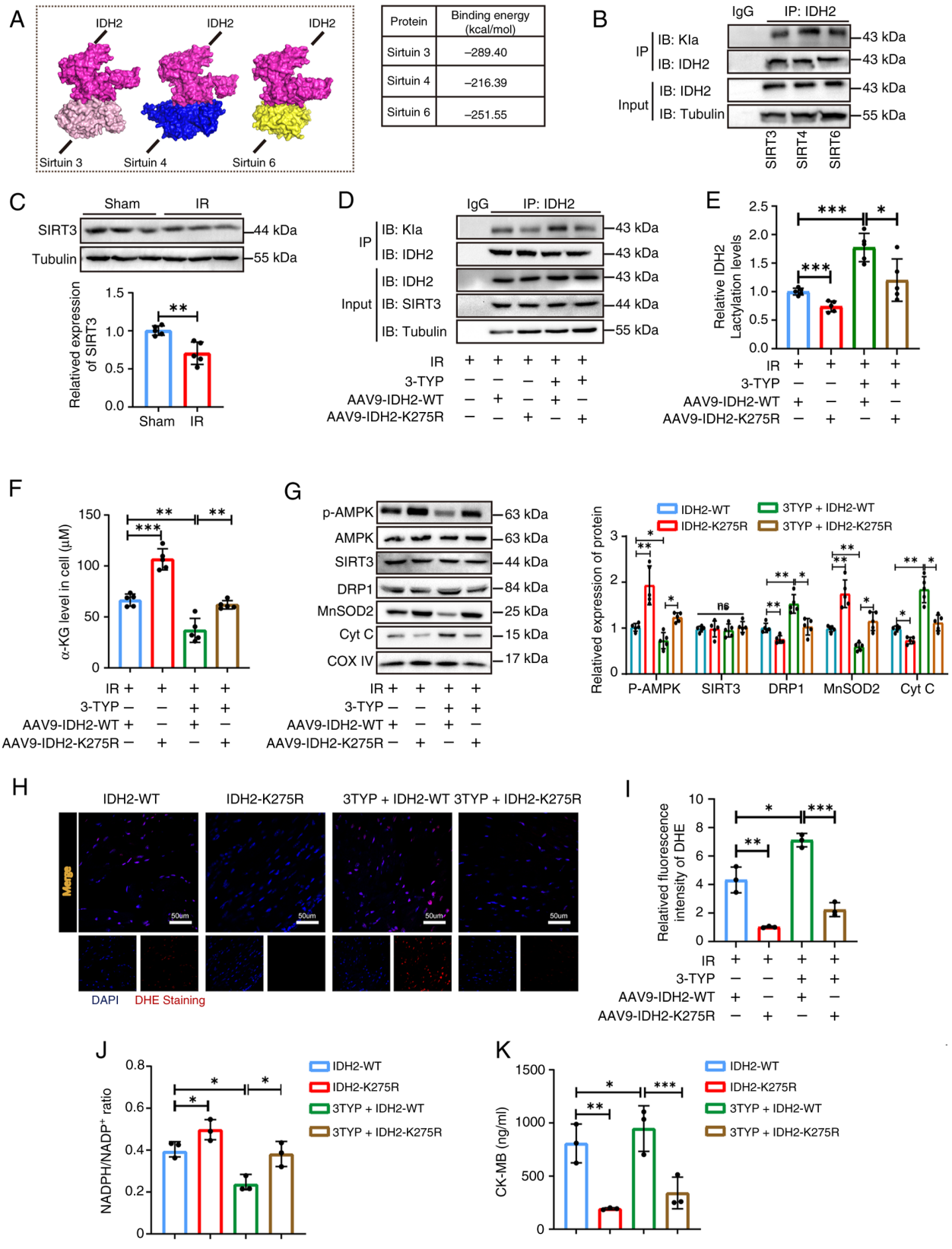

Figure 7. SIRT3 regulates myocardial oxidative injury by delactylating IDH2 in MIRI. (A) IDH2 docked with SIRT3, SIRT4, and SIRT6 molecules, respectively. (B) The level of IDH2 lactylation detected by IP assay after overexpressing SIRT3, SIRT4, SIRT6 (n=5). (C) SIRT3 protein expression levels in MIRI detected by western blot (n=5). (D and E) The level of IDH2 lactylation detected by IP experiment and semi-quantitative analyses (n=5). (F) α-KG production under 3-TYP treatment (n=5). (G) Protein levels of p-AMPK, AMPK, DRP1, MnSOD2 and Cyt C assayed by western blotting after 3-TYP treatment, and their semi-quantitative analyses (n=5). (H and I) Representative images of DHE staining for 3-TYP treatment group (n=5). (J and K) The NADPH/NADP$^+$ ratio and CK-MB levels in the 3-TYP treatment group (n=5). These data were representative results of three repetitions at least. Data are expressed as the mean ± SD. *P<0.05, **P<0.01 and ***P<0.001. IDH2, isocitrate dehydrogenase 2; MIRI, myocardial ischemia-reperfusion injury; IP, immunoprecipitation; 3-TYP, 3-(1H-1,2,3-Triazol-4-yl) pyridine; α-KG, α-ketoglutaric acid; p-, phosphorylated; AMPK, adenosine 5'-monophosphate-activated protein kinase; DRP1, dynamin-related protein 1; MnSOD2, manganese superoxide dismutase 2; Cyt C, cytochrome C; CK, creatine kinase; WT, wild-type; I/R, ischemia/reperfusion.

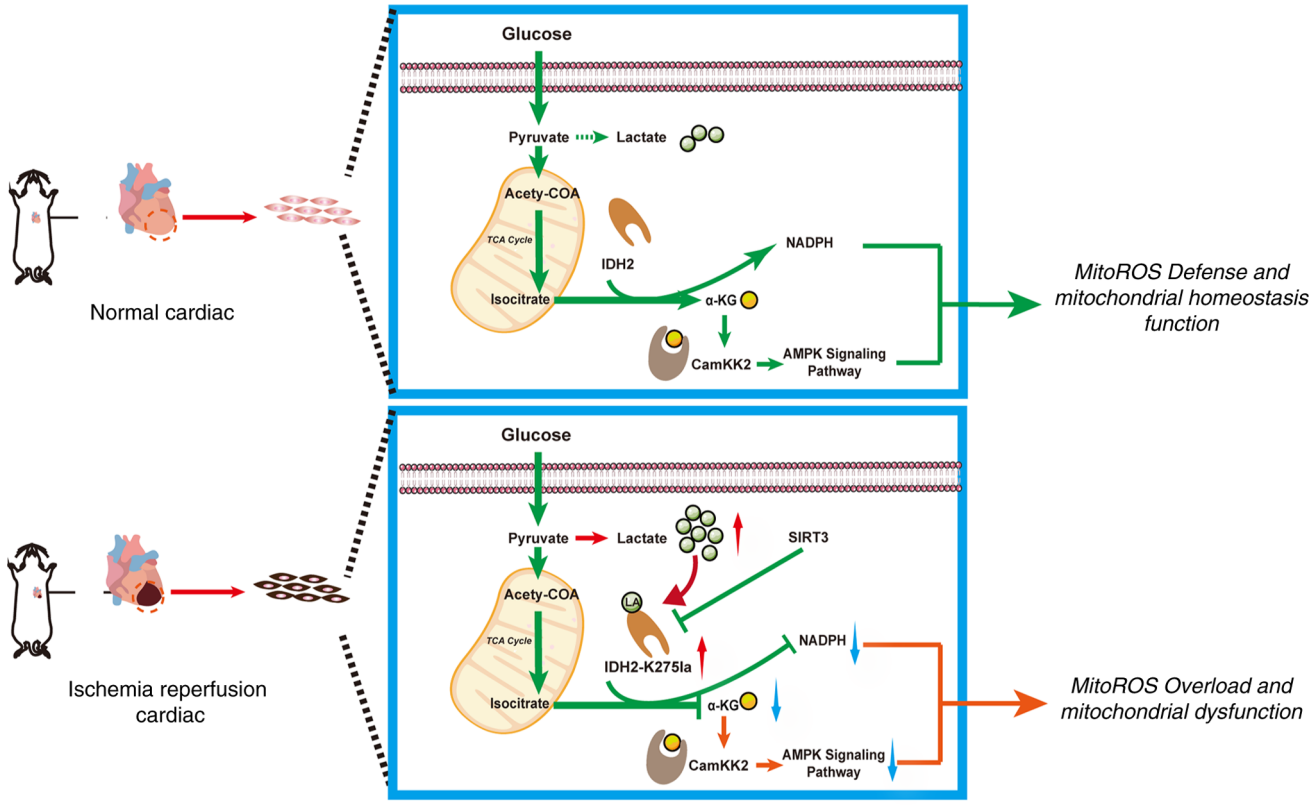

Figure 8. Schematic model of IDH2 lactylation in MIRI pathogenesis. Under physiological conditions, cardiac lactate does not accumulate excessively, and IDH2 lactylation remains at a basal level. This preserves IDH2 enzymatic activity, allowing it to maintain mitochondrial functional homeostasis and protect against oxidative stress. However, during MIRI, elevated intracellular lactate drives hyper-lactylation of IDH2. This aberrant modification impairs IDH2 function, disrupting downstream α-KG production and AMPK pathway activation. Consequently, mitochondrial dysfunction ensues, leading to myocardial damage and loss of cardiac function. Importantly, delactylating the IDH2-K275 site to reduce its lactylation can restore IDH2 activity, preserve mitochondrial homeostasis, and ultimately mitigate cardiac injury. IDH2, isocitrate dehydrogenase 2; myocardial ischemia-reperfusion injury; α-KG, α-ketoglutaric acid; AMPK, adenosine 5'-monophosphate-activated protein kinase; ROS, reactive oxygen species; TCA, tricarboxylic acid.

Protein lactylation is regulated by enzymes that often govern other lysine acylation such as p300/CBP and HDACs. It has been previously reported that SIRT1 and SIRT3 are 'erasers' of histone and non-histone Kla, with distinct regulatory mechanisms and substrate specificities (41). Previous studies have demonstrated that SIRT3, an NAD^+-dependent deacetylase, is vital for regulating cellular metabolism, stress reaction and organismal longevity (42,43). SIRT3 plays a key role in maintaining mitochondrial homeostasis. It regulates the deacylation of mitochondrial proteins and affects the activity of enzymes involved in important metabolic pathways, including fatty acid oxidation, the TCA cycle and OXPHOS (44,45). SIRT3 affects mitochondrial dynamics and biogenesis, and controls redox homeostasis. These processes are crucial for sustaining mitochondrial morphology, function and distribution. Studies have demonstrated that SIRT3 can regulate PGC-1-α, a protein implicated in neurodegenerative and cardiovascular diseases (46,47), increasing mitochondrial biogenesis and ensuring an adequate supply of functional mitochondria. Furthermore, SIRT3 is involved in mitophagy by regulating the expression and activity of PINK1/Parkin (48). SIRT3, a crucial cellular deacylation enzyme, reverses various lysine acylations, including acetylation, crotonylation, β-hydroxybutyrylation and propionylation (49,50). In terms of mitochondrial oxidative stress, SIRT3 can directly deacetylate and activate SOD2, thereby enhancing mitochondrial ROS scavenging and protecting them from oxidative damage. The present findings indicate that SIRT3 binds to IDH2 K275, acting as a regulator of IDH2 lactylation and IDH2 activity in MIRI, thereby affecting mitochondrial function. Significant downregulation of SIRT3 was found in MIRI, consistent with other studies. IDH2 K275 mutation can reverse mitochondrial dysfunction and reduce ROS production after SIRT3 inhibition. The downregulation of SIRT3 may be attributed to oxygen and nutrient deficiencies during the ischemic phase, leading to metabolic shifts that favor lactylation. However, whether SIRT3 knockdown initiates the enhanced lactylation of IDH2 during IR remains unclear. Whether corresponding molecular drugs that act on IDH2-K275 and effectively inhibit its lactylation are available remains a key focus of our subsequent research and clinical translation. It has been recently demonstrated that SIRT3 can be activated by salvianolic acid B, which directly deacetylates and activates superoxide dismutase and inhibits NLRP3 inflammasome activation by regulating mitochondrial ROS levels, thereby alleviating the inflammatory response accompanied by oxidative stress, which may affect IDH2 lactylation (51). Although salvianolic acid B has been reported to regulate histone lactylation, it is unknown whether it can regulate non-histone proteins. Follow-up studies are being conducted, and relevant experiments are being designed to validate our conjecture regarding salvianolic acid B and expect new findings.

The present study has several limitations. First, the regulation of SIRT3-mediated IDH2 lactylation was verified *in vivo* but not validated in cellular studies. Second, the precise mechanisms driving lactate elevation in MIRI have not been explored. Third, the present study did not explore the overexpression of SIRT3 in cellular or mouse models to determine whether it can prevent I/R-induced increase in IDH2 lactylation. Future studies should consider introducing overexpression vectors for verification. Moreover, the downstream consequences of reduced α-KG levels beyond AMPK inhibition require further investigation. Furthermore, the current lactylome data revealed other significantly modified proteins (for instance, ALDOA and NDUFS1) involved in metabolism and mitochondrial electron transport, whose roles in MIRI merit further study. From a therapeutic perspective, modern drug discovery increasingly focuses on small molecules that directly modulate specific PTMs (such as phosphorylation, acetylation and ubiquitination). Therefore, identifying a small-molecule compound that selectively targets the IDH2 K275 site to inhibit lactylation represents a promising strategy for clinical translation.

As illustrated in the mechanistic diagram (Fig. 8), sufficient evidence is provided that lactate elevations inhibit mitochondrial IDH2 function by modulating lactate levels in IDH2 K275 after myocardial I/R, which affects the production of the downstream metabolite α-KG, thereby affecting the activation of the AMPK pathway. The downregulation levels of SIRT3 in MIRI limit IDH2 K275 delactylation and further aggravated mitochondrial dysfunction in cardiomyocytes. Thus, future research should investigate diagnosis and treatment methods using this novel target.

Acknowledgements

The authors would like to thank the experimental facility of the Affiliated Hospital of Guangdong Medical University for help in the use of confocal microscopy and flow cytometry; Dr Li Xu (Affiliated Second Hospital of Guangdong Medical University, Zhanjiang, China) and Professor Jing Tang (Affiliated Hospital of Guangdong Medical University, Zhanjiang, China) for support and discussion during the present study.

Funding

The present study was supported by the Natural Science Foundation of Guangdong (grant no. 2022A1515012103), the Natural Science Foundation of Guangdong (grant no. 2024A1515013119) and the National Natural Science Foundation of China (grant no. 82370281).

Availability of data and materials

The data generated in the present study are included in the figures and/or tables of this article.

The data generated in the present study may be found in the ProteomeXchange under accession number PXD076346 or at the following URL: https://proteomecentral.proteomexchange.org/ui?view=datasets&search=PXD076346; and in the National Genomics Data Center under accession number OMIX015583 or at the following URL: https://ngdc.cncb.ac.cn/search/specific?db=omix&q=OMIX015583.

Authors' contributions

LQZ led the project. CSW and SMS designed and conceived the study. CSW, JDL, LX and SMS drafted the manuscript. LX and CSW performed data analysis. LX and CSW wrote, reviewed and edited the manuscript. SYCh, SYCa, SML and JNC fed the experimental mice. CSW, SYCh and JDL performed the animal experiments. ZQY and KD performed cell cultures. SYCa, LX and LQZ revised the manuscript. CSW, JDL and XDY performed the functional experiments. CSW and LQZ confirm the authenticity of all the raw data. All authors read and approved the final version of the manuscript.

Ethics approval and consent to participate

The ethics approval (approval no. AHGDMU-LAC-B-202301-0004) for animal research was obtained from the Experimental Animal Ethics Committee of Guangdong Medical University (Zhanjiang, China).

Patient consent for publication

Not applicable.

Competing interests

The authors declare that they have no competing interests.

References

1. Benjamin EJ, Blaha MJ, Chiuve SE, Cushman M, Das SR, Deo R, de Ferranti SD, Floyd J, Fornage M, Gillespie C, *et al*: Heart disease and stroke Statistics-2017 update: A report from the American heart association. Circulation 135: e146-e603, 2017.
2. Yellon DM and Hausenloy DJ: Myocardial reperfusion injury. N Engl J Med 357: 1121-1135, 2007.
3. Heusch G: Myocardial ischaemia-reperfusion injury and cardioprotection in perspective. Nat Rev Cardiol 17: 773-789, 2020.
4. Chan DC: Mitochondrial dynamics and its involvement in disease. Annu Rev Pathol 15: 235-259, 2020.
5. Dambrova M, Zuurbier CJ, Borutaite V, Liepinsh E and Makrecka-Kuka M: Energy substrate metabolism and mitochondrial oxidative stress in cardiac ischemia/reperfusion injury. Free Radic Biol Med 165: 24-37, 2021.
6. Ruiz-Meana M, Fernandez-Sanz C and Garcia-Dorado D: The SR-mitochondria interaction: A new player in cardiac pathophysiology. Cardiovasc Res 88: 30-39, 2010.
7. Wang Y and Patti GJ: The Warburg effect: A signature of mitochondrial overload. Trends Cell Biol 33: 1014-1020, 2023.
8. Quinn WJ III, Jiao J, TeSlaa T, Stadanlick J, Wang Z, Wang L, Akimova T, Angelin A, Schäfer PM, Cully MD, *et al*: Lactate limits T cell proliferation via the NAD(H) redox state. Cell Rep 33: 108500, 2020.
9. Bohn T, Rapp S, Luther N, Klein M, Bruehl TJ, Kojima N, Aranda Lopez P, Hahlbrock J, Muth S, Endo S, *et al*: Tumor immunoevasion via acidosis-dependent induction of regulatory tumor-associated macrophages. Nat Immunol 19: 1319-1329, 2018.
10. Yang X, Lu Y, Hang J, Zhang J, Zhang T, Huo Y, Liu J, Lai S, Luo D, Wang L, *et al*: Lactate-modulated immunosuppression of Myeloid-derived suppressor cells contributes to the radioresistance of pancreatic cancer. Cancer Immunol Res 8: 1440-1451, 2020.

11. Vaupel P, Schmidberger H and Mayer A: The Warburg effect: Essential part of metabolic reprogramming and central contributor to cancer progression. Int J Radiat Biol 95: 912-919, 2019.
12. Mao Y, Zhang J, Zhou Q, He X, Zheng Z, Wei Y, Zhou K, Lin Y, Yu H, Zhang H, *et al*: Hypoxia induces mitochondrial protein lactylation to limit oxidative phosphorylation. Cell Res 34: 13-30, 2024.
13. Zhang D, Tang Z, Huang H, Zhou G, Cui C, Weng Y, Liu W, Kim S, Lee S, Perez-Neut M, *et al*: Metabolic regulation of gene expression by histone lactylation. Nature 574: 575-580, 2019.
14. Xiong J, He J, Zhu J, Pan J, Liao W, Ye H, Wang H, Song Y, Du Y, Cui B, *et al*: Lactylation-driven METTL3-mediated RNA m6A modification promotes immunosuppression of tumor-infiltrating myeloid cells. Mol Cell 82: 1660-1677.e10, 2022.
15. Yang K, Fan M, Wang X, Xu J, Wang Y, Tu F, Gill PS, Ha T, Liu L, Williams DL and Li C: Lactate promotes macrophage HMGB1 lactylation, acetylation, and exosomal release in polymicrobial sepsis. Cell Death Differ 29: 133-146, 2022.
16. She H, Hu Y, Zhao G, Du Y, Wu Y, Chen W, Li Y, Wang Y, Tan L, Zhou Y, *et al*: Dexmedetomidine ameliorates myocardial Ischemia-reperfusion injury by inhibiting MDH2 lactylation via regulating metabolic reprogramming. Adv Sci (Weinh) 11: e2409499, 2024.
17. Leary S, Underwood W, Anthony R, Cartner S, Grandin T, Greenacre C, Gwaltney-Brant S, Ann McCrackin M, Meyer R, Miller D, *et al*: AVMA Guidelines for the Euthanasia of Animals: 2020 Edition. Schaumburg, IL, American Veterinary Medical Association, 2020.
18. Ehler E, Moore-Morris T and Lange S: Isolation and culture of neonatal mouse cardiomyocytes. J Vis Exp: 50154, 2013 doi: 10.3791/50154.
19. Rigaud VOC, Hoy RC, Kurian J, Zarka C, Behanan M, Brosious I, Pennise J, Patel T, Wang T, Johnson J, *et al*: RNA-Binding Protein LIN28a regulates new myocyte formation in the heart through long noncoding RNA-H19. Circulation 147: 324-337, 2023.
20. Jin L, Chun J, Pan C, Kumar A, Zhang G, Ha Y, Li D, Alesi GN, Kang Y, Zhou L, *et al*: The PLAG1-GDH1 axis promotes anoikis resistance and tumor metastasis through CamKK2-AMPK signaling in LKB1-Deficient lung cancer. Mol Cell 69: 87-99.e87, 2018.
21. Sun L, Zhang Y, Yang B, Sun S, Zhang P, Luo Z, Feng T, Cui Z, Zhu T, Li Y, *et al*: Lactylation of METTL16 promotes cuproptosis via m6A-modification on FDX1 mRNA in gastric cancer. Nat Commun 14: 6523, 2023.
22. Ma L, Shi H, Li Y, Gao W, Guo J, Zhu J, Dong Z, Sun A, Zou Y and Ge J: Hypertrophic preconditioning attenuates myocardial ischemia/reperfusion injury through the deacetylation of isocitrate dehydrogenase 2. Sci Bull (Beijing) 66: 2099-2114, 2021.
23. Ørn S and van Hall G: Does a normal peripheral lactate value always indicate an aerobic tissue metabolism? Eur J Heart Fail 19: 1034-1035, 2017.
24. Bhattacharya B, Mohd Omar MF and Soong R: The Warburg effect and drug resistance. Br J Pharmacol 173: 970-979, 2016.
25. Li W, Zhou C, Yu L, Hou Z, Liu H, Kong L, Xu Y, He J, Lan J, Ou Q, *et al*: Tumor-derived lactate promotes resistance to bevacizumab treatment by facilitating autophagy enhancer protein RUBCNL expression through histone H3 lysine 18 lactylation (H3K18la) in colorectal cancer. Autophagy 20: 114-130, 2024.
26. Li F, Si W, Xia L, Yin D, Wei T, Tao M, Cui X, Yang J, Hong T and Wei R: Positive feedback regulation between glycolysis and histone lactylation drives oncogenesis in pancreatic ductal adenocarcinoma. Mol Cancer 23: 90, 2024.
27. Zhu Z, Huang C, Chen J, Wan L, Zhang C and Wang J: Lactylation at the crossroads of immune metabolism and epigenetic regulation: Revealing its role in rheumatic immune diseases. J Transl Med 24: 25, 2025.
28. Zhang N, Zhang Y, Xu J, Wang P, Wu B, Lu S, Lu X, You S, Huang X, Li M, *et al*: α-myosin heavy chain lactylation maintains sarcomeric structure and function and alleviates the development of heart failure. Cell Res 33: 679-698, 2023.
29. Wang J, Yang P, Yu T, Gao M, Liu D, Zhang J, Lu C, Chen X, Zhang X and Liu Y: Lactylation of PKM2 suppresses inflammatory metabolic adaptation in Pro-inflammatory macrophages. Int J Biol Sci 18: 6210-6225, 2022.
30. Wang H, Xiong Q, He G, Tang J, Sun L, Cheng S, Ke M, Chen S, Hu Y, Feng J, *et al*: Hepatic IDH2 regulates glycolysis and gluconeogenesis. Metabolism 143: 155559, 2023.
31. Zhang GF, Jensen MV, Gray SM, El K, Wang Y, Lu D, Becker TC, Campbell JE and Newgard CB: Reductive TCA cycle metabolism fuels glutamine- and glucose-stimulated insulin secretion. Cell Metab 33: 804-817.e5, 2021.
32. Kim H, Lee JH and Park JW: IDH2 deficiency exacerbates acetaminophen hepatotoxicity in mice via mitochondrial dysfunction-induced apoptosis. Biochim Biophys Acta Mol Basis Dis 1865: 2333-2341, 2019.
33. Barnabas GD, Lee JS, Shami T, Harel M, Beck L, Selitrennik M, Jerby-Arnon L, Erez N, Ruppin E and Geiger T: Serine biosynthesis is a metabolic vulnerability in IDH2-driven breast cancer progression. Cancer Res 81: 1443-1456, 2021.
34. Liu X and Gong Y: Isocitrate dehydrogenase inhibitors in acute myeloid leukemia. Biomark Res 7: 22, 2019.
35. Si X, Shao M, Teng X, Huang Y, Meng Y, Wu L, Wei J, Liu L, Gu T, Song J, *et al*: Mitochondrial isocitrate dehydrogenase impedes CAR T cell function by restraining antioxidant metabolism and histone acetylation. Cell Metab 36: 176-192.e10, 2024.
36. Han SJ, Choi HS, Kim JI, Park JW and Park KM: IDH2 deficiency increases the liver susceptibility to ischemia-reperfusion injury via increased mitochondrial oxidative injury. Redox Biol 14: 142-153, 2018.
37. Noh MR, Kong MJ, Han SJ and Park KM: Isocitrate dehydrogenase 2 deficiency aggravates prolonged high-fat diet intake-induced hypertension. Redox Biol 34: 101548, 2020.
38. Xu W, Yang H, Liu Y, Yang Y, Wang P, Kim SH, Ito S, Yang C, Wang P, Xiao MT, *et al*: Oncometabolite 2-hydroxyglutarate is a competitive inhibitor of α-ketoglutarate-dependent dioxygenases. Cancer Cell 19: 17-30, 2011.
39. Stein EM, DiNardo CD, Pollyea DA, Fathi AT, Roboz GJ, Altman JK, Stone RM, DeAngelo DJ, Levine RL, Flinn IW, *et al*: Enasidenib in mutant IDH2 relapsed or refractory acute myeloid leukemia. Blood 130: 722-731, 2017.
40. Mellinghoff IK, van den Bent MJ, Blumenthal DT, Touat M, Peters KB, Clarke J, Mendez J, Yust-Katz S, Welsh L, Mason WP, *et al*: Vorasidenib in IDH1- or IDH2-Mutant Low-Grade Glioma. N Engl J Med 389: 589-601, 2023.
41. Du R, Gao Y, Yan C, Ren X, Qi S, Liu G, Guo X, Song X, Wang H, Rao J, *et al*: Sirtuin 1/sirtuin 3 are robust lysine delactylases and sirtuin 1-mediated delactylation regulates glycolysis. iScience 27: 110911, 2024.
42. Morigi M, Perico L and Benigni A: Sirtuins in renal health and disease. J Am Soc Nephrol 29: 1799-1809, 2018.
43. Gong Y, Tang N, Liu P, Sun Y, Lu S, Liu W, Tan L, Song C, Qiu X, Liao Y, *et al*: Newcastle disease virus degrades SIRT3 via PINK1-PRKN-dependent mitophagy to reprogram energy metabolism in infected cells. Autophagy 18: 1503-1521, 2022.
44. Kim TS, Jin YB, Kim YS, Sun Y, Lu S, Liu W, Tan L, Song C, Qiu X, Liao Y, *et al*: SIRT3 promotes antimycobacterial defenses by coordinating mitochondrial and autophagic functions. Autophagy 15: 1356-1375, 2019.
45. Li Z, Hu O, Xu S, Lin C, Yu W, Ma D, Lu J and Liu P: The SIRT3-ATAD3A axis regulates MAM dynamics and mitochondrial calcium homeostasis in cardiac hypertrophy. Int J Biol Sci 20: 831-847, 2024.
46. Ding Y, Yang H, Wang Y, Chen J, Ji Z and Sun H: Sirtuin 3 is required for osteogenic differentiation through maintenance of PGC-1α-SOD2-mediated regulation of mitochondrial function. Int J Biol Sci 13: 254-264, 2017.
47. Gao J, Zhang K, Wang Y, Guo R, Liu H, Jia C, Sun X, Wu C, Wang W, Du J and Chen J: A machine learning-driven study indicates emodin improves cardiac hypertrophy by modulation of mitochondrial SIRT3 signaling. Pharmacol Res 155: 104739, 2020.
48. Long D, Deng Z, Zhao X, Xu Y, Li W, Mo X, Zhong Y, Li M, He A, Zhang Z, *et al*: m7G-modified mt-tRF3b-LeuTAA regulates mitophagy and metabolic reprogramming via SUMOylation of SIRT3 in chondrocytes. Biomaterials 314: 122903, 2025.
49. Li R, Yan L, Sun X and Zheng W: A bicyclic pentapeptide-based highly potent and selective pan-SIRT1/2/3 inhibitor harboring Nε-thioacetyl-lysine. Bioorg Med Chem 28: 115356, 2020.
50. Zhang X, Cao R, Niu J, Yang S, Ma H, Zhao S and Li H: Molecular basis for hierarchical histone de-β-hydroxybutyrylation by SIRT3. Cell Discov 5: 35, 2019.
51. Wei XH, Chen J, Wu XF, Zhang Q, Xia GY, Chu XY, Xia H, Lin S and Shang HC: Salvianolic acid B alleviated myocardial ischemia-reperfusion injury via modulating SIRT3-mediated crosstalk between mitochondrial ROS and NLRP3. Phytomedicine 136: 156260, 2025.